

Chapter IV

Redox behavior of copper and zinc dimers supported by
bis(2-diisobutylphosphino-4-*t*-butylphenyl)amido ligands[†]

[†]Adapted from Harkins, S. B.; Peters, J. C.; Amido-bridged Cu₂N₂ diamond core complexes in three oxidation states. *J. Am. Chem. Soc.*, to be submitted for publication.

IV.A. Introduction

Research concerning the magnetic and spectroscopic properties of dicopper complexes is perhaps the most widely studied topic in bimetallic transition metal chemistry.¹ This interest derives from their role in enzymatic processes or for their potential use as photosensitizers, organic light emitting devices (OLEDs), and molecular magnets.^{2,3} The ability of dicopper complexes to mediate multi-electron transfer processes and/or small molecule activation is a related concept. In order to realize such chemical transformations using bimetallic copper/ligand systems, complexes which can support two-electron redox processes need to be developed. Further, it is likely that for systems of this nature to be efficient, or even possible, the bimetallic copper complexes would have to resist major structural reorganization during electron-transfer processes. This idea, so termed the “entatic state,” has been found repeatedly in nature as mechanisms of small molecule activation and electron transfer in metalloproteins are probed.⁴ An excellent example of this phenomenon is in the metalloenzyme nitrous oxide reductase(N₂OR).⁵ This dimeric protein catalyzes the two electron, reduction of N₂O to N₂ and H₂O, and is facilitated through a synergistic process involving a tetranuclear Cu₄S functional site (Cu_Z) and a Cu₂S₂ electron transfer site (Cu_A). In another example, particulate methane monooxygenase (pMMO) catalyzes the two electron oxidation of methane to methanol using a combination of mono- and dicopper cofactors.⁶ Interestingly, the copper-catalyzed chemical transformations observed in N₂OR and pMMO have never been demonstrated in small molecule copper chemistry, but both are thought to involve dicopper sites which minimize structural reorganization.

Typically, the redox states of dicopper systems have been investigated in the context of understanding enzymatic processes. The dicopper site of N₂OR and cytochrome *c* oxidase are excellent illustrations of this.^{5b,7,8} Because of interest in understanding the Cu_A cofactor, numerous mixed-valence dicopper complexes have been synthesized over the last 30 years in an effort to probe the intramolecular electron transfer properties of the two copper nuclei.^{9,10,11,12} Hundreds more dicopper(II,II) complexes have been prepared in a variety of studies, and have been found to primarily occur in square-planar or trigonal bipyramidal coordination geometries. While the field of dicopper chemistry has been extensively explored for a variety of oxidation states and gives rise to various types of magnetic interactions, a single dicopper system which can be isolated in each of three oxidation states has not been reported. Over fifteen years ago, Holm and co-workers first demonstrated this concept of low structural reorganization in a small molecule across three oxidation states with a bimetallic iron system.¹³ In that system, an Fe₂(OR)₂ diamond-core complex was found in isostructural environments for the Fe^{II}Fe^{II}, Fe^{II}Fe^{III}, and Fe^{III}Fe^{III} oxidation states where the Fe-centers were constrained in octahedral geometries. Similar systems containing Cu have not been previously described, likely due to the tendency of the copper nuclei to distort and bind additional ligands upon oxidation thus hampering the reversibility of multi-electron redox processes.

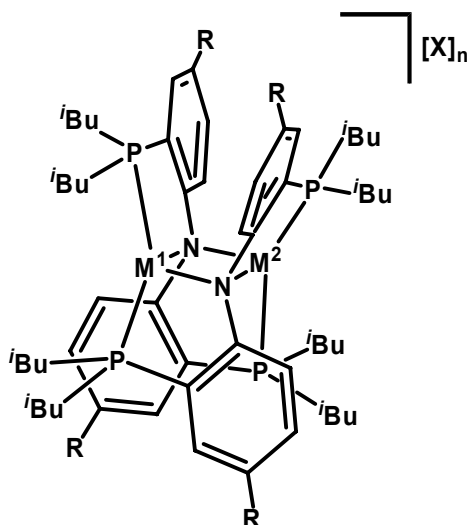
Luminescent, polymetallic copper complexes are also well known and though they have been studied for many years on a variety of ligand platforms, advances continue to be made.^{14,15} They are almost exclusively cationic in nature and exhibit emissive lifetimes of ~100 ns – 10 μs.^{16,17} Distortion of the typical tetrahedral geometry of Cu^I towards square-planar upon photoexcitation requires a considerable amount of

reorganization energy and is problematic when attempting to design highly emissive complexes.¹⁸ As a result of this geometry change in the excited state, quenching due to exciplex formation is also common. Systems where structural reorganization in the excited state has been minimized and where the Cu centers are sterically protected from solvent coordination, not surprisingly exhibit the highest quantum yields.¹⁹ Despite the vast number of complexes that have been prepared in order to study both rapid electron transfer and luminescence phenomena, a single system which exhibits both these characteristics through low-structural reorganization has yet to be reported. With this concepts in mind, a novel family of Cu₂N₂ complexes have been developed.

Initially work was focused on the synthesis and characterization of a dinuclear, thioether-supported Cu₂N₂ complex $\{(SNS)Cu^I\}_2$ ($[SNS]^- = \text{bis}(2\text{-tert-butylsulfanylphenyl})\text{amide}$).²⁰ This compound is characterized by a Cu₂N₂ diamond core configuration in which two d^{10} Cu centers are bridged by two diaryl-amido linkages. Oxidation of $\{(SNS)Cu^I\}_2$ affords the class III,²¹ fully-delocalized dicopper cation, $[\{(SNS)Cu^{1.5}\}_2]^+$. A key feature of this initial system was the observation of very minimal structural reorganization between oxidation states. However, upon oxidation of $\{(SNS)Cu^I\}_2$ to $[\{(SNS)Cu^{1.5}\}_2]^+$, a ~ 0.13 Å contraction in the Cu \cdots Cu distance from 2.599 Å to 2.472 Å was observed.²² It is important to note that these minor perturbations to the core atoms occur in the absence of additional ligand coordination or significant topological reorganization, thus functionally modeling the electron transfer process of the Cu_A site. As expected from the small structural reorganization upon oxidation from $\{(SNS)Cu^I\}_2$ to $[\{(SNS)Cu^{1.5}\}_2]^+$, the electron self-exchange process between the two redox forms is very fast and a rate constant of $k_s > 10^7$ M⁻¹s⁻¹ was estimated. A higher

potential irreversible wave which was speculated to be an unstable dicopper(II,II) species was also observed.

Building on these studies, our current efforts have been devoted to stabilizing the second oxidation process of a Cu_2N_2 diamond core complex. The problem was addressed by replacing the *t*-butyl thioether chelates with more reducing diisobutylphosphine groups. This change was found to be both sterically and electronically beneficial, affording the Cu_2N_2 complex $\{(\text{PNP})\text{Cu}\}_2$ (**4.3**) which does exhibit two reversible one-electron redox transitions by cyclic voltammetry. In the current manuscript, this chemistry has been elaborated by the preparation of a family of bimetallic copper and zinc complexes supported by $[\text{PNP}]^-$ type ligands (PNP = bis(2-(diisobutylphosphino)-phenyl)amide, **4.1**; *t*-Bu₂-PNP = bis(2-(diisobutylphosphino)-4-*t*-butylphenyl)amide, **4.4**) (Figure IV.1). These molecules are characterized by amido-bridged Cu_2N_2 diamond core geometries, where the chelating phosphines of one ligand coordinate to two different copper nuclei. The fully-reduced dicopper complexes, **4.3** and **4.5** are exceptionally luminescent at room temperature. One electron chemical oxidation of either **4.3** or **4.5** results in the fully delocalized class III mixed valence $\text{Cu}^{1.5}\text{N}_2$ diamond core complexes, **4.8** and **4.10**, respectively. Though the two electron chemical oxidation of **4.3** results in decomposition, further oxidation of **4.5** results in the paramagnetic, dicationic dimer **4.11**. The solid-state molecular structures of the bimetallic complexes have been determined and are presented along with spectroscopic and magnetic studies. Interestingly, structural, spectroscopic and magnetic studies of **4.11** also provides evidence for a resonance stabilized paramagnetic Cu^{III} center in a pseudo-tetrahedral geometry.



- 4.2: $M^1 = \text{Li}$ $M^2 = \text{Li}$ $R = \text{H}$
 4.3: $M^1 = \text{Cu}^{\text{I}}$ $M^2 = \text{Cu}^{\text{I}}$ $R = \text{H}$
 4.5: $M^1 = \text{Cu}^{\text{I}}$ $M^2 = \text{Cu}^{\text{I}}$ $R = \text{tBu}$
 4.6a: $M^1 = \text{Zn}^{\text{II}}$ $M^2 = \text{Zn}^{\text{II}}$ $R = \text{tBu}$ $X = \text{PF}_6$ $n = 2$
 4.6b: $M^1 = \text{Zn}^{\text{II}}$ $M^2 = \text{Zn}^{\text{II}}$ $R = \text{tBu}$ $X = \text{OTf}$ $n = 2$
 4.7: $M^1 = \text{Cu}^{\text{I}}$ $M^2 = \text{Zn}^{\text{II}}$ $R = \text{tBu}$ $X = \text{PF}_6$ $n = 1$
 4.8: $M^1 = \text{Cu}^{1.5}$ $M^2 = \text{Cu}^{1.5}$ $R = \text{H}$ $X = \text{BAr}^{\text{F}}$ $n = 1$
 4.10a: $M^1 = \text{Cu}^{1.5}$ $M^2 = \text{Cu}^{1.5}$ $R = \text{tBu}$ $X = \text{BAr}^{\text{F}}$ $n = 1$
 4.10b: $M^1 = \text{Cu}^{1.5}$ $M^2 = \text{Cu}^{1.5}$ $R = \text{tBu}$ $X = \text{SbF}_6$ $n = 1$
 4.11: $M^1 = \text{Cu}^{\text{I}}$ $M^2 = \text{Cu}^{\text{III}}$ $R = \text{tBu}$ $X = \text{SbF}_6$ $n = 2$

Figure IV.1: Representative dimer of M_2N_2 complexes ($\text{BAr}^{\text{F}} = [\text{B}(\text{C}_6\text{H}_3(\text{CF}_3)_2)_4]$).

To our knowledge, the presented system is the first example of a dicopper system which can stabilize two successive one electron oxidations without deviating from a pseudo-tetrahedral geometry around the Cu centers. The collective characterization data presented herein all support the assignment of a highly covalent Cu_2N_2 structure, which through electronic delocalization is able to minimize structural reorganization across different electronic environments, thus mimicking the behavior of dicopper active sites in enzymes.

IV.B. Results and Discussion

IV.B.1. Diamagnetic complexes 4.1-4.7

Preparation of bimetallic, d^{10} complexes supported by PNP-type ligands. The ligand (PNP)H, **4.1**, was prepared in good yield by metathesis of 2,2'-difluorophenylamine with two equivalents of $(\text{iBu})_2\text{PLi}$ in THF. Following quenching of the reaction with methanol and work-up, **4.1** was afforded as a pale green oil. In order to develop a useful metathesis reagent for metallation, **4.1** was deprotonated with $^n\text{BuLi}$ in

petroleum ether which afforded the lithium dimer, $\{(PNP)Li\}_2$ (**4.2**) as a light yellow powder. Dimeric **4.2** is analogous to the previously reported $\{(BQA)Li\}_2$,²³ and does not form $(PNP)Li(\text{solvent})_2$ -type complexes²⁴ when prepared in hydrocarbon solvents. Metathesis of **4.2** with $(Me_2S)CuBr$ in benzene immediately forms the dicopper complex **4.3** in nearly quantitative yield with concomitant loss of $LiBr$. Complex **4.3** is bright yellow and is characterized by a single resonance in its ^{31}P NMR spectrum (-33.9 ppm) and exceptional luminescence in fluid solution at room temperature as we have previously communicated.

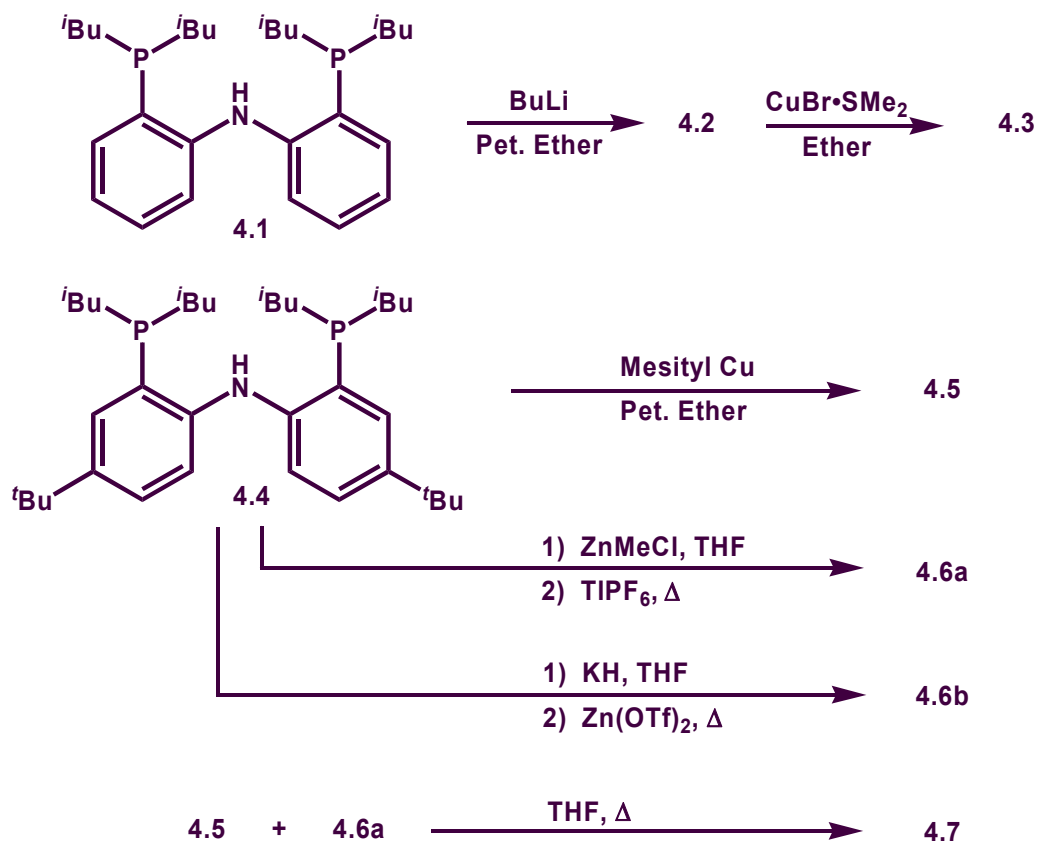


Figure IV.2: Synthesis of complexes **4.2**, **4.3**, **4.5**, **4.6**, and **4.7**.

The current work describes the synthesis of a family of dimeric complexes where the ligand has been derivatized with a *t*-butyl group in the 4-position of the aryl ring. This

substitution was accomplished following methodology recently published by Ozerov and co-workers for the synthesis of PNP-type ligands.²⁵ In our preparation, di(2-bromo-4-^tbutylphenyl)amine was treated with three equivalents of ⁿbutyl lithium in diethyl ether which lithiates the 2-positions of the aryl rings and deprotonates the amine. Subsequent addition of three equivalents of diisobutylchlorophosphine to the reaction mixture affords the tris(phosphine) substituted product after 36 h. The P-N bond can be readily cleaved with anhydrous HCl in ether which affords the desired ligand **4.4** as a white solid following work-up. Experimentally it has been determined that it is necessary to use ≥ 3 equivalents of diisobutylchlorophosphine to achieve the desired product. The first two equivalents metathesize with the amide and one of the aryl ring positions and do not undergo further rearrangement. This is in contrast to the synthesis reported by Ozerov, where diisopropylchlorophosphine reportedly undergoes the same substitution, but then migrates from the amide to the other aryl ring positions. This process does not occur in our system even with prolonged reaction times and elevated temperatures. We attribute this phenomenon to the decreased steric interaction between the diisobutylphosphine groups of the amide and the aryl ring compared to those interactions between diisopropylphosphine groups.

In order to avoid the synthesis of lithiated **4.4** because of difficulties with isolation, a different route to metallation was pursued. Metathesis of amine ligands with mesityl copper is a well established route to achieve amido-copper complexes.²⁶ Effective metallation of **4.4** was achieved with mesityl copper in petroleum ether over a period of 12 h which afforded the copper dimer, $\{({}^t\text{Bu}_2\text{-PNP})\text{Cu}\}_2$ (**4.5**) in high yield upon work-up. Complex **4.5** is characterized as a luminescent yellow solid that is extremely soluble

in solvents such as petroleum ether and hexamethyldisiloxane but negligibly soluble in acetonitrile. A single resonance in the ^{31}P NMR spectrum of **4.5** is observable at -35.3 ppm and is shifted upfield of **4.3**, consistent with the more electron-rich phosphorus nuclei. Despite the presence of eight isobutyl and four t -butyl groups per dimeric molecule, the complex is highly crystalline allowing the growth of X-ray quality crystals by slow evaporation of a concentrated solution of **4.5** in THF.

To enhance our understanding of the spectroscopic and electrochemical characteristics of **4.3** and **4.5**, the Zn_2N_2 dimer was synthesized. This was accomplished by addition of a solution of MeZnCl in THF to a solution of **4.4**, which after heating for 4 h was treated with TIPF_6 . Heating was continued for 16 h and after work-up [$\{({}^t\text{Bu}_2\text{-PNP})\text{Zn}\}_2][\text{PF}_6]_2$ (**4.6a**) was isolated in modest yield as a white solid. Complex **4.6a** is poorly soluble in THF once isolated, but can be crystallized from methylene chloride/petroleum ether. Because X-ray quality crystals of **4.6a** could not be attained, the analogous triflate ($[\text{OTf}]^-$) salt was synthesized. Reaction of **4.4** with KH in THF followed by addition of $\text{Zn}(\text{OTf})_2$ and refluxing for 24 h afforded **4.6b** which was found to be spectroscopically identical to **4.6a**. Crystals suitable for X-ray diffraction were obtained by cooling a concentrated solution of **4.6b** in methylene chloride/petroleum ether to $-35\text{ }^\circ\text{C}$.

The mixed-metal CuZnN_2 dimer was also prepared. Conveniently, combination of **4.6a** and **4.5** in THF quantitatively results in [$\{({}^t\text{Bu}_2\text{-PNP})\text{Cu}\}\{({}^t\text{Bu}_2\text{-PNP})\text{Zn}\}][\text{PF}_6]$, **4.7**, after refluxing for 18 h in THF as determined by ^{31}P NMR. The product was isolated as X-ray quality pale yellow crystals from THF/petroleum ether. The mixed metal formulation of crystalline **4.7** was assigned based on two resonances in the ^{31}P NMR

which are shifted slightly from the starting materials and are approximately equal in integration. The resonance in the ^{31}P NMR spectrum at -31.8 ppm is assigned to the Cu coordinated phosphine atoms, which is broadened relative to the resonance at -40.0 ppm assigned to the Zn coordinated phosphines as a result of the large quadrupolar moment of copper.²⁷

X-ray diffraction studies. To examine the structural impact of metal substitution on the dimer conformation, the solid-state molecular structures of the d^{10} complexes **4.2**, **4.5**, **4.6** and **4.7** have been solved and are detailed in Table IV.1. The X-ray diffraction study of **4.3** has been previously reported and the relevant bond lengths and angle measurements are also included in Table IV.1. Characteristic to all five complexes is the four-component, M_2N_2 diamond core structural arrangement formed by two metal atoms and two bridging amide nitrogen atoms. The metal atoms are additionally supported by two phosphine ligands which gives rise to the compressed tetrahedral geometry about each copper center and to the overall D_2 molecular symmetry. In these closed-shell species, the intermetallic distances range from 2.4680(27)Å to 2.8826(3)Å and support N-M-N angles from 107.23(9)° to 92.93(6)° which is illustrative of the plasticity which can be supported while maintaining the dimeric conformation.

The structure of **4.2** was determined and from this the similarity to $\{(\text{BQA})\text{Li}\}_2$ was confirmed. A short $\text{Li}(1)\cdots\text{Li}(2)$ distance of 2.4680(27) Å is found, which results from the short M-N bond distances of average 2.07 ± 0.01 Å as a result of the high ionic character of the bonds. This is the shortest intermetallic distance in the presented series, though it is somewhat longer than the $\text{Li}(1)\cdots\text{Li}(2)$ distance reported for $\{(\text{BQA})\text{Li}\}_2$

Table IV.1: Core structural representations (50% probability ellipsoids), selected bond lengths (Å) and angles (deg.) for **4.2**, **4.3**, **4.5**, **4.6b**, and **4.7**.

	4.2 ^a	4.3 ^b	4.5 ^b	4.6b ^c	4.7 ^d
M(1)-M(2)	2.4680(27)	2.6245(8)	2.7283(7)	2.8826(3)	2.7518(5)
M(1)-N(1)	2.074(2)	2.127(4)	2.164(3)	2.0931(16)	2.114(2)
M(1)-N(2)	2.062(2)	2.191(4)	2.139(3)	2.0933(16)	2.159(2)
M(2)-N(1)	2.066(2)	2.179(4)	2.135(3)	2.0805(16)	2.112(2)
M(2)-N(2)	2.087(2)	2.219(4)	2.173(3)	2.1071(17)	2.121(2)
M(1)-P(1)	2.5126(19)	2.2173(13)	2.2326(13)	2.3250(5)	2.2851(7)
M(1)-P(4)	2.5309(19)	2.2339(13)	2.2439(13)	2.3350(6)	2.2744(7)
M(2)-P(2)	2.5437(19)	2.2241(13)	2.2236(13)	2.3515(5)	2.3033(7)
M(2)-P(3)	2.5333(19)	2.2235(13)	2.2139(13)	2.3457(5)	2.3080(8)
N(1)-M(1)-N(2)	107.23(9)	107.20(14)	101.35(11)	92.97(6)	98.58(9)
N(1)-M(2)-N(2)	106.57(9)	104.44(14)	101.19(11)	92.93(6)	99.84(9)
M(1)-N(1)-M(2)	73.18(8)	75.10(12)	78.77(10)	87.37(6)	81.25(8)
M(1)-N(2)-M(2)	73.01(8)	73.03(12)	78.52(10)	86.67(6)	80.02(7)
P(1)-M(1)-P(4)	139.50(8)	132.93(5)	136.36(4)	139.31(2)	139.77(3)
P(2)-M(2)-P(3)	140.47(8)	137.69(5)	139.27(5)	141.92(2)	141.08(3)

Notes *a*: M(1), M(2) = Li; *b*: M(1), M(2) = Cu; *c*: M(1), M(2) = Zn; *d*: M(1) = Cu, M(2) = Zn

(2.395(5)). This robust structural configuration also gives rise to the thermal stability of **4.2** which is not typically expected for lithium amides.

The structure of **4.3** is very analogous to **4.2**, though a longer intermetallic distance of 2.6245(8) Å and longer M-N bond lengths, 2.18 ± 0.04 Å (av.), are observed. Shortened M-P bonds of 2.23 ± 0.01 Å reflect the increased covalent character of copper compared to that of lithium. Interestingly, four-coordinate Li^{I} (0.59 Å) and Cu^{I} (0.60 Å) are reported to have the same ionic radii²⁸ and would not inherently suggest an increased bonding radius when they have the same charge. We attribute the overall core expansion to the repulsion between anti-bonding Cu-Cu *d*-orbitals interaction which exists in **4.3**, but is absent between the lithium atoms of **4.2**.

While complexes **4.2** and **4.3** were the subject of our initial inquiry, the major aspect of the current work will focus on those metal complexes supported by the 'butyl substituted ligand **4.4**. The solid-state molecular structures of **4.5** is very similar to that of **4.3** in that the Cu-N/Cu-P differ only slightly: 2.15 ± 0.02 Å/ 2.23 ± 0.01 Å for **4.5** and 2.18 ± 0.04 Å/ 2.23 ± 0.01 Å for **4.3** on average. The key differences lie in the N-M-N angles which are compressed by 4.6° in **4.5** relative to **4.3**; this results in the 0.1 Å expansion of the Cu(1)⋯Cu(2) distance. This expansion is likely due to the increased electron density at the Cu_2N_2 core which creates more repulsion between the Cu *d*- and N *p*-orbitals. The increase in electron density is expected with the addition of electron donating 'butyl groups to the aryl rings. These structural changes are considered to be purely an electronic consequence, as no steric interactions associated with 'butyl group are evident from the crystal structure.

The dizinc complex, **4.6b**, adopts the same diamond core configuration as the Li and Cu dimers described above. This isostructural relationship was expected because four-coordinate Zn^{II} is also reported to have the same ionic radius as Cu^I (0.60 Å) and is isoelectronic with **4.5**. Dimer **4.6b** exhibits the longest M...M distance (2.8826(3) Å) of the M_2N_2 systems studied thus far. Shortening of the M-N bonds by ~0.06 Å and elongation of the M-P bonds by ~0.11 Å in **4.6b** compared to **4.5** is also observed. This substantial core expansion is reasonably attributed to the inherent cationic repulsion between the Zn^{2+} ions. It is also likely that this repulsion allows for the formation **4.7** by redistribution between **4.6b** with **4.5**. In other respects the structure of **4.6** is generally unremarkable and is effectively isostructural with **4.5**.

X-ray diffraction study of the $CuZnN_2$ dimer **4.7** indicates similarities to both of its homo-dimer parents **4.5** and **4.6b**. The presence of a single PF_6 anion in the asymmetric unit is in agreement with the monocationic, mixed metal formulation of **4.7**. The internuclear $Cu\cdots Zn$ distance of 2.7518(5) Å is intermediate in length between the 2.7283(7) Å intermetallic distance of **4.5** and the 2.8826(3) Å distance observed in **4.6b**. Crystallographically, the copper and zinc atoms are indistinguishable from each other given their nuclear similarity. For the purpose of structural refinement the Cu and Zn atoms have been assigned as indicated in Table IV.1, which was based on bond length similarities between the structure of **4.7** and those of **4.5** and **6**. No comparable internal differences in the M-N bond lengths could be correlated as being N-Cu or N-Zn in parentage, consistent with the notion of a large degree of electronic delocalization across the M_2N_2 diamond core. However, differences in the M-P bond lengths did prove to be diagnostic. The M(1)-P bond lengths were found to be ~1% shorter than the M(2)-P bond

lengths on average suggesting that M(1) is primarily Cu in the crystal lattice, and M(2) is primarily Zn. However, given the structural homogeneity between the two metal sites, it is impossible to know the precise percentage of each individual metal at either site. The crystal structure does, however, confirm the presumed isostructural identity of **4.7** to the other systems studied.

Optical Spectroscopy. The absorption spectra of **4.2** in benzene and **4.3** in THF solution are shown in Figure IV.3 (top). Complex **4.2** exhibits two prominent absorption bands with $\lambda_{\text{max}} = 303 \text{ nm}$ ($\epsilon 18\,200 \text{ M}^{-1}\text{cm}^{-1}$) and 359 nm ($\epsilon 17\,200 \text{ M}^{-1}\text{cm}^{-1}$), and shoulders at 398 nm and 414 nm which gives rise to the pale yellow color. Complex **4.3** has an intense charge-transfer band with $\lambda_{\text{max}} = 350 \text{ nm}$ ($\epsilon 42\,000 \text{ M}^{-1}\text{cm}^{-1}$), which is not as prominent in the spectrum of **4.2**. Peaks with $\lambda_{\text{max}} = 423 \text{ nm}$ ($\epsilon 4400 \text{ M}^{-1}\text{cm}^{-1}$) and a shoulder at $\sim 446 \text{ nm}$ have been assigned as the MLCT transitions which are typical for Cu^{I} complexes and result in the intense yellow color.

The absorption spectra for **4.5**, **4.6a**, and **4.7** were also collected and plotted in Figure IV.3 (bottom). The Zn_2N_2 dimer, **4.6**, absorbs strongly at 302 nm ($\epsilon 30\,500 \text{ M}^{-1}\text{cm}^{-1}$) with shoulders at 327 nm and 344 nm . As expected, **4.6** appears essentially unchanged from the ligand (**4.4**) absorption spectra which exhibits a maxima at 302 nm ($\epsilon 18\,700 \text{ M}^{-1}\text{cm}^{-1}$) and a shoulder at 334 nm . Conversely, the Cu_2N_2 dimer, **4.5**, has a much richer spectroscopic signature characterized by ligand absorption bands at 295 nm ($\epsilon 20\,500 \text{ M}^{-1}\text{cm}^{-1}$) and 318 nm ($\epsilon 21\,100 \text{ M}^{-1}\text{cm}^{-1}$) and a more intense band at 352 nm ($\epsilon 33\,300 \text{ M}^{-1}\text{cm}^{-1}$) with a shoulder at 383 nm . The spectrum of **4.5** also has two characteristic MLCT bands at 433 nm ($\epsilon 4600 \text{ M}^{-1}\text{cm}^{-1}$) and 459 nm ($\epsilon 3800 \text{ M}^{-1}\text{cm}^{-1}$), which appear at slightly lower energy of the corresponding bands in **4.3** as result of increased electron density at the

metal center. The intense band at 302 nm is assigned to the metal-metal 3d→4p transition based on the assignments made by Che and Miskowski on related luminescent Cu^I-Cu^I dimers.²⁹ The related band is also present in the spectrum of **4.3** at 350nm which is notably shifted to lower energy of **4.5** by ~4500 cm⁻¹. This assignment is supported by the fact that this transition is not observed in **4.7** which has absorption maxima associated with ligand-based transitions at 290 nm (ϵ 21 600 M⁻¹ cm⁻¹), 306 nm (ϵ 23 400 M⁻¹ cm⁻¹), and 350 nm (sh). A broad MLCT transition centered at 396 nm (ϵ 7400 M⁻¹ cm⁻¹) is also evident though it shifted to higher energy than the MLCT bands observed in the spectrum of **4.5**.

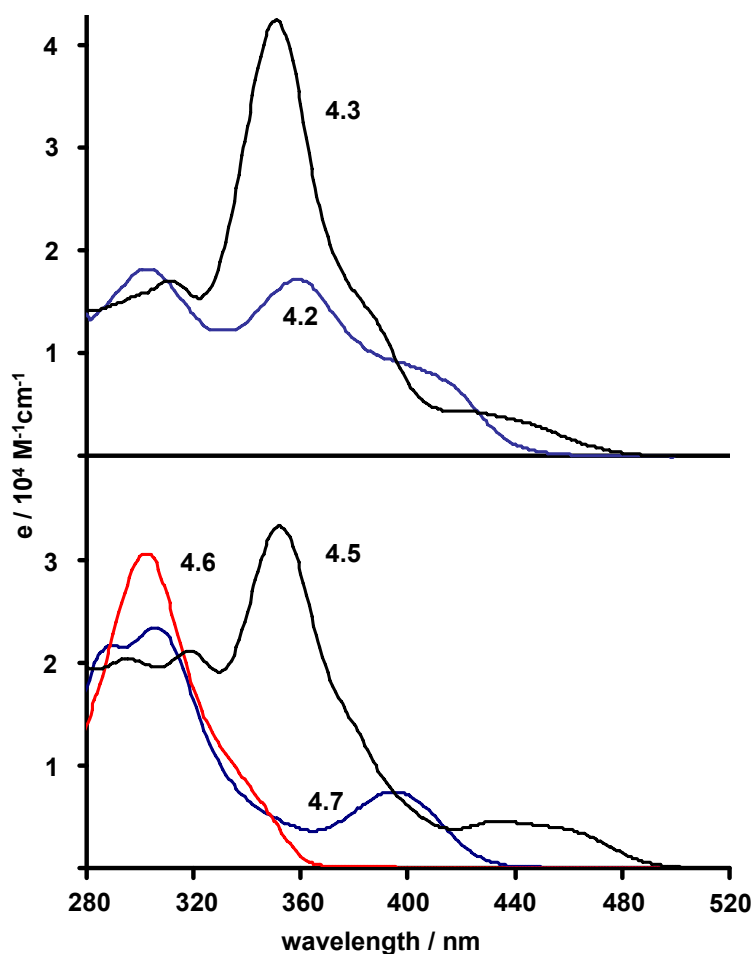


Figure IV.3: Absorption spectra. *Top:* **4.2** (blue) in benzene and **4.3** (black) in THF. *Bottom:* **4.5** (black), **4.6** (red) and **4.7** (blue) in THF.

Electrochemistry. The initial motivation for this study was spurred by the observation of a pseudo-reversible $\text{Cu}^{\text{II}}\text{Cu}^{\text{II}}/\text{Cu}^{1.5}\text{Cu}^{1.5}$ wave in an $\{(\text{SNS})\text{Cu}\}_2$ copper dimer at $E_{\text{pa}} = +0.57$ V (0.35 M [TBA][PF₆] in THF). It was hypothesized that by moving from thioether chelates to stronger donating phosphine ligands that this higher potential redox couple would become fully reversible. The electrochemistry of complexes **4.3**, **4.5**, **4.6**, and **4.7** was studied by cyclic voltammetry and the traces are plotted in Figure IV.4.³⁰ The dicopper dimers, **4.3** and **4.5**, display two cleanly reversible one electron redox processes. The low potential processes at -0.405 V and -0.490 V, for **4.3** and **4.5** respectively, is assigned to the $\text{Cu}^{1.5}\text{Cu}^{1.5}/\text{Cu}^{\text{I}}\text{Cu}^{\text{I}}$ transition based on previous studies. As a result of switching from thioether to more strongly reducing phosphine chelates, the potential has been substantially shifted to lower potential from the $\{(\text{SNS})\text{Cu}\}_2$ $\text{Cu}^{1.5}\text{Cu}^{1.5}/\text{Cu}^{\text{I}}\text{Cu}^{\text{I}}$ redox couple ($E_{1/2} = -0.250$ mV). Higher potential waves were observed at $+0.295$ V and $+0.210$ V for **4.3** and **4.5** respectively.

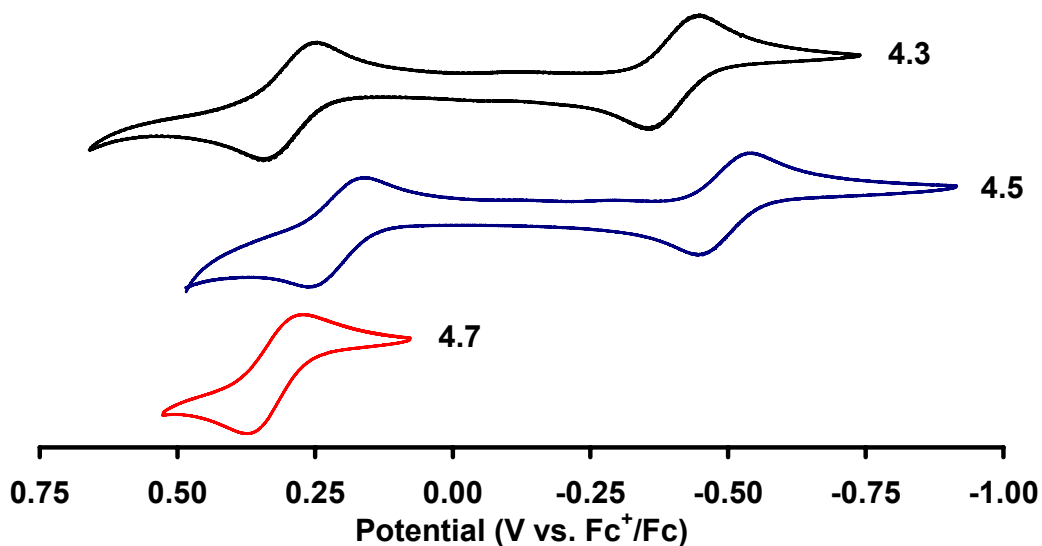


Figure IV.4: Cyclic Voltammetry of **4.3** (black), **4.5** (blue), and **4.7** (red) in 0.35 M [TBA][PF₆] in THF

As a result of installing an electron-donating, ^tbutyl group to the aryl ring, both redox processes have been shifted to lower potential by 85 mV in **4.5** relative to **4.3**. This is consistent with the copper centers being more electron rich and therefore harder to reduce. Interestingly, both redox processes are shifted together, suggesting that the redox processes are directly linked to redox processes involving one or both of the copper nuclei rather than simply oxidation of the ligand. Given that both redox processes are now observable on the electrochemical time-scale the electronic structure of the double oxidized species is clearly of interest.

With complexes **4.6a** and **4.7** in hand their cyclic voltammetry was also probed. The dizinc dimer, **4.4**, showed no electrochemical events in the window (CH₂Cl₂) from +0.80 to -2.00 V vs. Fc⁺/Fc, which is typical for Zn complexes. This observation suggests strongly against the possibility of a pure ligand radical corresponding to the higher potential wave of either **4.3** or **4.5**. The mixed-metal dimer, **4.7**, shows no redox processes at potentials similar to those of the Cu^{1.5}Cu^{1.5}/Cu^ICu^I transitions, though a single reversible wave at +0.320 V is apparent. This electrochemical event is shifted 110 mV positive of the high potential wave of **4.5**. As both **4.5** and **4.7** are isostructural, bimetallic *d*¹⁰ systems, it is reasonable to consider that they are resulting from the same electronic transition and the shifting of **4.7** to higher potential is associated with the cationic charge which is not present in **4.5**.

Emission Spectroscopy. The emission properties of complexes **4.2–4.5** have been examined in fluid solution. Complexes **4.3** and **4.5** have similar emission spectra centered at 500 nm and 511 nm, respectively, with negligible changes in the full-width at half-max. Given the relatively small change in the Hammett parameter (σ), by switching

from H- to ^tBu- on the aryl ring, the red-shifted maximum is considerable³¹ thus presenting the possibility for tuning the emissive properties. The lifetime (τ) and quantum yield (ϕ) of **4.5** were determined ($\tau = 11.4 \mu\text{s}$ and $\phi = 0.58$) comparable to **4.3** ($\tau = 10.9 \mu\text{s}$, $\phi = 0.67$).

We also attempted to study the photophysics of complexes **4.6a** and **4.7**. The dizinc complex, **4.6a**, is negligibly emissive and difficult to distinguish from trace impurities. However, complex **4.7** did have a weak, but resolvable, emission profile in dichloromethane centered at 455 nm ($\phi \sim 7 \times 10^{-4}$) with a lifetime of $\tau \leq 500$ ps which is reminiscent of other mononuclear copper luminophores. From this data, it is evident that the dicopper interaction is essential in order to achieve long-lived excited states on this particular molecular scaffold. A reasonable explanation is that the dicopper complexes **4.3** and **4.5** are better able to stabilize the excited state by delocalizing the unpaired electron across the Cu_2N_2 core. This is based on the suggestions that the excited state molecules are similar to the one-electron oxidized species, **4.8** and **4.10**. Whether this excited state delocalization necessitates a direct Cu-Cu bond, or a *cuprophilic* interaction, is yet to be established. We do suggest however that the intense emission observed for **4.3** and **4.5**, but not for **4.6** and **4.7**, results from excitation into the $3d \rightarrow 4p$ or $3d \rightarrow 4s$ transition owing to the uniqueness of the Cu_2N_2 system.

Interestingly, the lithium dimer, **4.2**, has a uncommonly large quantum yield ($\phi = 0.45$) with a emission decay that is 1000 times faster ($\tau \sim 4$ ns) than that observed for **4.3**. Also, the emission spectrum is broader and the nonradiative decay rate is $\sim 1 \times 10^4$ times larger than **4.3** and **4.5** which suggests that different electronic states are involved. A

possible explanation for the high quantum yield is that lithium atoms constrict the organic framework in a rigid environment similar to other organic fluorophores.

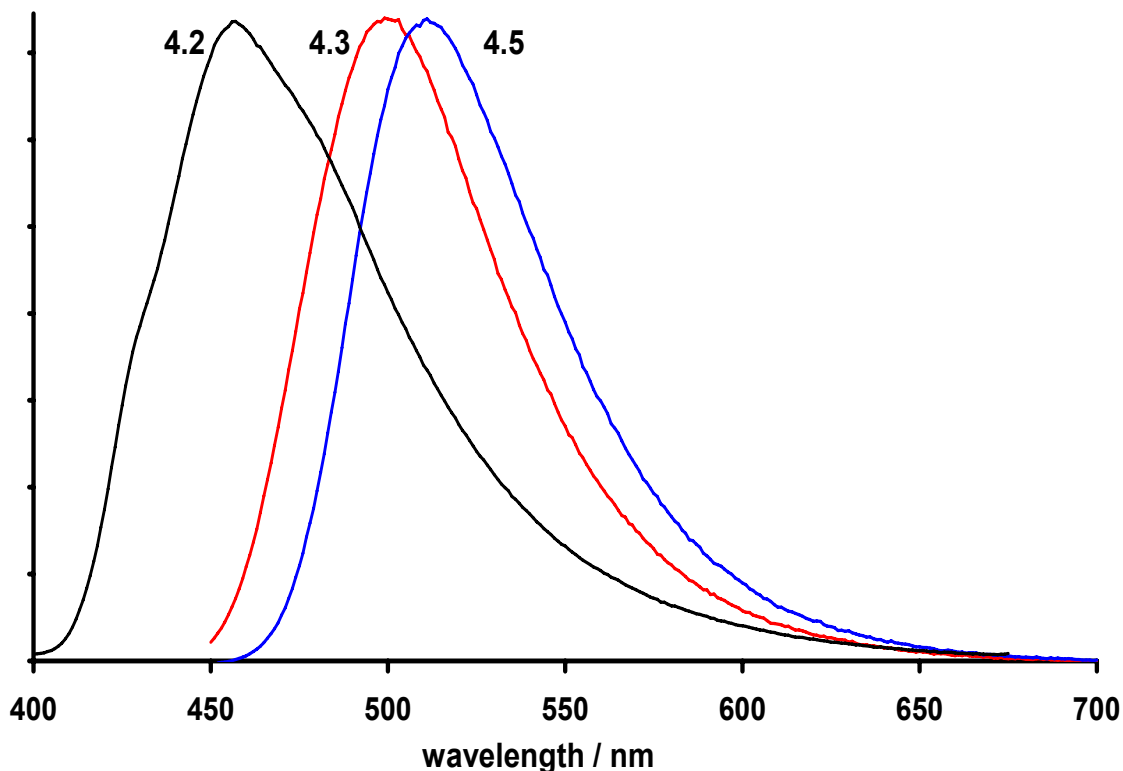


Figure IV.5: Emission spectrum of complexes **4.2**, **4.3**, and **4.5** (intensity is not reflective of quantum yield).

IV.B.2. Paramagnetic complexes 4.8-4.11

Oxidative Synthesis of 4.8-4.11. Based on the electrochemical studies of the d^{10} complexes and our prior success in isolating the one-electron oxidation products of Cu_2N_2 complexes supported by the $[\text{SNS}]^-$ ligand, the chemical oxidations of **4.3** and **4.5** were pursued. Addition of one equivalent of $[\text{Cp}_2\text{Fe}][\text{B}(\text{C}_6\text{H}_3(\text{CF}_3)_2)_4]$ to **4.3** in dichloromethane immediately induces a color change from brilliant yellow to deep red and affords the one electron oxidized product, **4.8**, as red-brown prisms following work-up and recrystallization from diethyl ether/petroleum ether. The paramagnetic complex

4.8 was found to contain a 1:1 ratio of dimer to counterion by elemental analysis consistent with the mixed-valence assignment.

The two electron oxidation of **4.3** was also attempted. Reaction of **4.3** with two equivalents [NO][BF₄] in either dichloromethane or chlorobenzene resulted in the darkening of the yellow solution to red, consistent the intermediate formation of the mono-oxidized complex **4.8**.³² Within minutes, the solution became blue in color and in approximately 30 min had converted to an inky violet-colored homogeneous solution. Isolation and characterization of the product, **4.9**, proved arduous. The violet solid, which results from removal of the solvent *in vacuo*, is only compatible with halogenated solvents as it is insoluble in non-polar solvents such as ether and benzene, and is decomposed by any donor solvents (THF³³, CH₃CN, or trace H₂O). Product isolation was ultimately achieved by recrystallization of **4.9** from chlorobenzene/petroleum ether which afforded green crystals that are purple as an amorphous powder. Microanalysis indicated 1:1:1 relationship of [4.1]⁻:Cu:BF₄ which was consistent with the desired doubly oxidized dimeric product of **4.3**. The ¹H and ³¹P NMR spectra of crystalline **4.9** were indicative of a diamagnetic product which was completely dissimilar from the spectrum of **4.3**. The ¹⁹F NMR spectrum of **4.9** contained a broad bimodal signal from the BF₄ counterion and is indicative of fluxional interaction with the Cu nuclei and is also evident from the multiple broad signals observed in the ¹H and ³¹P NMR spectra.

The solid-state molecular structure of **4.9** was determined by X-ray diffraction. The crystallized product, which is the majority (> 90%) based on absorption spectroscopy, is actually a ligand-fused decomposition product which results presumably from intermolecular radical coupling (Figure IV.6). In the asymmetric unit (triclinic, P-1)

there are two unconnected copper containing half-molecules which are related by inversion through the newly formed C=C bond between the aryl rings. Two BF₄ counterions, and two chlorobenzene solvent molecules were also found in the asymmetric unit, neither of which are associated with the copper atoms in the solid state (closest contacts: Cl...Cu 9.269(9) Å; F...Cu 11.896(3) Å). The bond order assigned in the schematic of **4.9** (Figure IV.6) is based the crystallographically determined bond lengths and on an assignment of a Cu^I oxidation state based on its coordination geometry and molecular diamagnetism. This high degree of π -conjugation gives rise to intense absorption band at 613 nm (ϵ 16 250 M⁻¹cm⁻¹) and results in the inky violet color. Molecules that display this type of conjugation have been previously reported by Hammond and are spectroscopically similar to **4.9**.³⁴ From these studies, **4.9** can be described as a Cu^I cation coordinated by a neutral η^3 -ligand in a t-shaped geometry which explains its facile decomposition in coordinating solvents. The presence of the chlorobenzene solvent molecules in the crystals lattice also explains why crystallization was only accomplished in this solvent. We theorize that **4.9** results from an intermolecular coupling between two [$\{(PNP)Cu\}_2$]²⁺ with reductive loss of H₂, which results from radical character at the 4-position of the aryl rings. Despite evidence for the isostructural two electron oxidation product of **4.3** as an intermediate in the synthesis of **4.9** based on the color transitions and the reversibility of the electrochemical redox processes, further attempts to isolate the dimeric intermediate were not pursued.

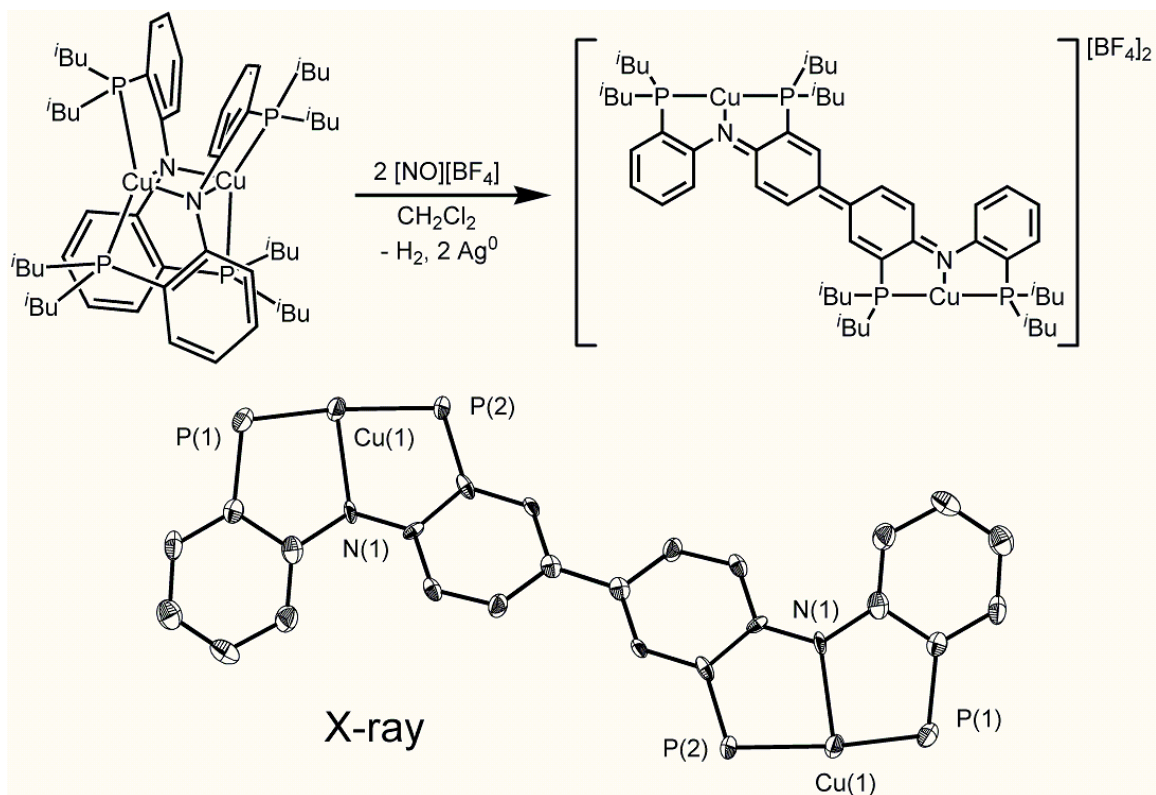


Figure IV.6: *Top*, Decomposition of **4.3** upon two electron oxidation. *Bottom*, Solid-state molecular structure (50% probability ellipsoids) of **4.9** (isobutyl groups, solvent molecules, and anions omitted for clarity). Selected bond lengths (Å) and angles (deg.): Cu(1)-N(1), 2.108(6); Cu(1)-P(1), 2.212(2); Cu(1)-P(2), 2.212(2); N(1)-Cu(1)-P(1), 86.29(18); N(1)-Cu(1)-P(2), 86.07(18); P(1)-Cu(1)-P(2), 167.55(8).

The observation of **4.9** was the initial impetus for the synthesis of ligand **4.4**, which was designed to prevent the observed radical coupling mechanism. It has been well-documented that installing *i*butyl groups on aryl rings of semiquinonates can help stabilize resonance radicals at those positions.³⁵ Reaction of **4.5** with [Cp₂Fe][B(C₆H₃(CF₃)₂)₄] in ether or AgSbF₆ in THF rapidly afforded the one electron oxidized $\{[(i\text{Bu})_2\text{-PNP}]\text{Cu}^{1.5}\}_2^+$ complexes **4.10a** and **4.10b**, respectively. Both complexes were obtained as red-brown crystalline solids in good yield upon recrystallization. Cation **4.10a** formed much larger crystals than **4.10b** presumably

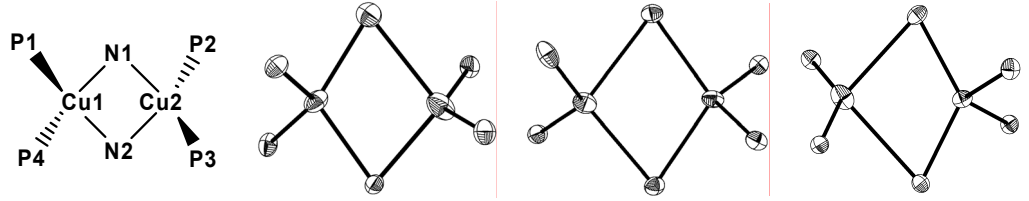
because of a more matched cation/anion packing. Microanalysis of both **4.10a** and **4.10b** found a 1:1 cation:anion ratio which is consistent with mixed valence assignment.

Addition of two equivalents of $[\text{NO}][\text{SbF}_6]$ to **4.5** dissolved in dichloromethane immediately resulted in the characteristic red color of **4.10b**, which progressed to deep blue over the course of 10 min. It is important to note that this is the identical reaction profile to what was observed for the early stages of two electron oxidation of **4.3**. In this case the inky violet color of the decomposition complex **4.9** was not observed even after stirring for several hours. Crude isolation of the two-electron oxidation product, **4.11**, as a blue solid was accomplished by removal of the solvent in vacuo. Multiple recrystallizations of **4.11** from dichloromethane/petroleum ether at $-35\text{ }^\circ\text{C}$ afforded analytically pure material in modest yield. Microanalysis indicated a precise 1:2 ratio of dimer to SbF_6 , thus confirming the two fold oxidation of **4.5** and the inherent dicationic nature of **4.11**. Similar to **4.9**, **4.11** is largely incompatible with coordinating solvents and is insoluble in hydrocarbons. Complex **4.11** is paramagnetic and characterization by NMR is not possible due to the large quadrupolar moment of the copper nuclei. The paramagnetic behavior of **4.11** was initially surprising because of the presumed proximity of the copper nuclei in the dimer. With the short $\text{Cu}\cdots\text{Cu}$ distances afforded by this ligand scaffold and the ability of the Cu_2N_2 core to delocalize electron density, antiferromagnetic coupling between unpaired spins and thus room temperature diamagnetism was expected, and not observed.

Crystallographic Studies. The solid-state molecular structures of all oxidized species were determined by X-ray diffraction and the core representations with relevant bond lengths and angles are shown in Table IV.2. The mono-oxidized species **4.8** and

4.10a both exhibit pronounced contractions in the Cu(1)···Cu(2) distance of 0.08 Å and 0.20 Å respectively, compared to that observed in the Cu^ICu^I complexes **4.3** and **4.5** (Table IV.1). Comparable Cu-P bond lengths of 2.22-2.27 Å exist in both structures of **4.8** and **4.10a** and contain P-Cu-P bond angles of 133.4-140.8°. In comparing **4.8** and **4.10a** to **4.3** and **4.5**, it was found that the Cu-P bonds contract by 0.12 Å on average while P-Cu-P angles are essentially unchanged.

Table IV.2: Core structural representations (50% probability ellipsoids), selected bond lengths (Å) and angles (deg.) for **4.8**, **4.10a**, and **4.11**



	4.8	4.10a	4.11
M(1)-M(2)	2.5406(6)	2.5264(6)	2.5245(9)
M(1)-N(1)	2.0567(19)	2.148(3)	2.332(3)
M(1)-N(2)	2.0596(16)	2.206(3)	2.452(3)
M(1)-P(1)	2.2657(6)	2.2574(9)	2.2278(8)
M(1)-P(4)	2.2470(6)	2.2594(10)	2.2244(8)
M(2)-N(1)	2.3627(19)	2.061(3)	2.002(3)
M(2)-N(2)	2.0931(17)	2.059(3)	1.976(2)
M(2)-P(2)	2.2531(6)	2.2624(9)	2.2766(9)
M(2)-P(3)	2.2219(6)	2.2580(9)	2.2836(8)
N(1)-M(1)-N(2)	113.37(7)	102.03(10)	95.19(8)
N(1)-M(2)-N(2)	100.89(6)	110.50(10)	125.31(10)
M(1)-N(1)-M(2)	69.89(6)	73.75(8)	70.83(8)
M(1)-N(2)-M(2)	75.55(6)	72.56(8)	68.60(8)
P(1)-M(1)-P(4)	133.36(2)	136.13(4)	149.89(3)
P(2)-M(2)-P(3)	140.77(2)	133.91(4)	127.94(3)

More remarkable structural contortions are observable in the Cu₂N₂ diamond core construction. Unlike the highly symmetric Cu₂N₂ diamond core observed for [(SNS)Cu^{1.5}]⁺, larger deviations are observed in the systems presented here. Cation **4.8** contains three Cu-N bonds of ~2.07 Å and one of 2.3627(19) Å which facilitate the

contracted Cu(1)···Cu(2) distance of 2.5406(6) Å. Conversely, the solid-state structure of **4.10a** does not exhibit the same elongated Cu-N bond, but it still achieves a highly contracted Cu(1)···Cu(2) distance of 2.5264(6) Å. In this case, Cu(1) has Cu-N bond distances of 2.18 Å (ave.) and Cu(2) has Cu-N bond distances of 2.06 Å (av.) suggesting the possibility for electronic inequivalence between the copper centers. Despite the structural aberrations which are observable between **4.8** and **4.10a**, the overall trend of the Cu₂N₂ core contracting upon oxidation remains consistent, though the contraction from **4.5** to **4.10a** is more than twice that of **4.3** to **4.8**.

Finally, the deep blue crystalline complex, **4.11**, was studied by X-ray diffraction. Immediately upon inspection of the solid-state structure significant structural deviation from the mixed-valence complex **4.10a** is apparent. The first feature of interest is that the Cu(1)···Cu(2) distance of 2.5245(9) Å in **4.11** is unchanged from that of **4.10a**. While this bond length and overall ligand super-structure is unperturbed, significant inequivalence in the bonding environment at the Cu sites has resulted. At Cu(1), bonds to N(1) and N(2) of 2.332(3) Å and 2.452(3) Å, respectively, are observed and based on length suggest dative interactions between Cu(1) with both N atoms.³⁶ Cu(2), on the other hand, has comparatively short bonds to N(1) and N(2) of 2.002(3) Å and 1.976(2) Å indicative of metal-amide bonds and may be indicative of electronic inequivalence between the two Cu nuclei. The comparable Cu(1)-N(1)-Cu(2) and Cu(1)-N(2)-Cu(2) bond angles which result are illustrative of the conserved molecular symmetry despite changes in bonding at the individual copper nuclei. Changes to the electronic structure at the individual Cu nuclei is also evidenced by lengthening of the Cu-P bonds at Cu(2) to ~2.28 Å and shortening of the Cu-P bonds at Cu(1) to ~2.23 Å.³⁷

Magnetic Studies The X-band EPR spectrum of the mixed-valence complexes **4.8** and **4.10a** were obtained in 2-methyltetrahydrofuran at 3.7 K and are shown with their corresponding simulations in Figure IV.7. The data obtained are consistent with a class III delocalized mixed-valence species. The observed EPR signal of **4.8**, clearly displays a seven-line hyperfine coupling due to the interaction of a single unpaired electron delocalized over two Cu ($S=3/2$) nuclei. The hyperfine coupling is most clearly resolved in the g_z tensor, and spectrum can be adequately simulated with the following parameters: $g_x = 1.996$, $g_y = 2.020$, $g_z = 2.095$, $A_x = 9.5 \cdot 10^{-4} \text{ cm}^{-1}$, $A_y = 26 \cdot 10^{-4} \text{ cm}^{-1}$, $A_z = 28 \cdot 10^{-4} \text{ cm}^{-1}$. As with previous amido-dicopper system we have studied, the g_z tensor is located at a lower g -value than is typical of class III delocalized systems, and makes the precise hyperfine coupling assignment difficult in the absence of higher frequency (Q-band) experiments. Super-hyperfine coupling to the bridging nitrogen nuclei of the Cu_2N_2 core or to the phosphine chelates are also not discernable from these experiments. Cationic **4.10a** exhibits a very isotropic signal with poorly defined hyperfine coupling; these characteristics persisted regardless of the solvent compositions, temperature (3.7-100 K), or counter ion (**4.10b**) which were tried. The spectrum does however bear gross similarity to the spectrum of **4.8** and can be simulated using substantially large line-widths. The parameters used for the simulation shown in Figure IV.7 are $g_x = 1.987$, $g_y = 2.025$, $g_z = 2.098$, $A_x = 10.5 \cdot 10^{-4} \text{ cm}^{-1}$, $A_y = 20 \cdot 10^{-4} \text{ cm}^{-1}$, $A_z = 25 \cdot 10^{-4} \text{ cm}^{-1}$, which are very consistent with those obtained for the simulation of **4.8**. Based on these experiments we conclude that despite the odd structural distortions observed in the solid state, significant electronic delocalization in the Cu_2N_2 core persists in both molecules and that the class III assignment is fully consistent with data.

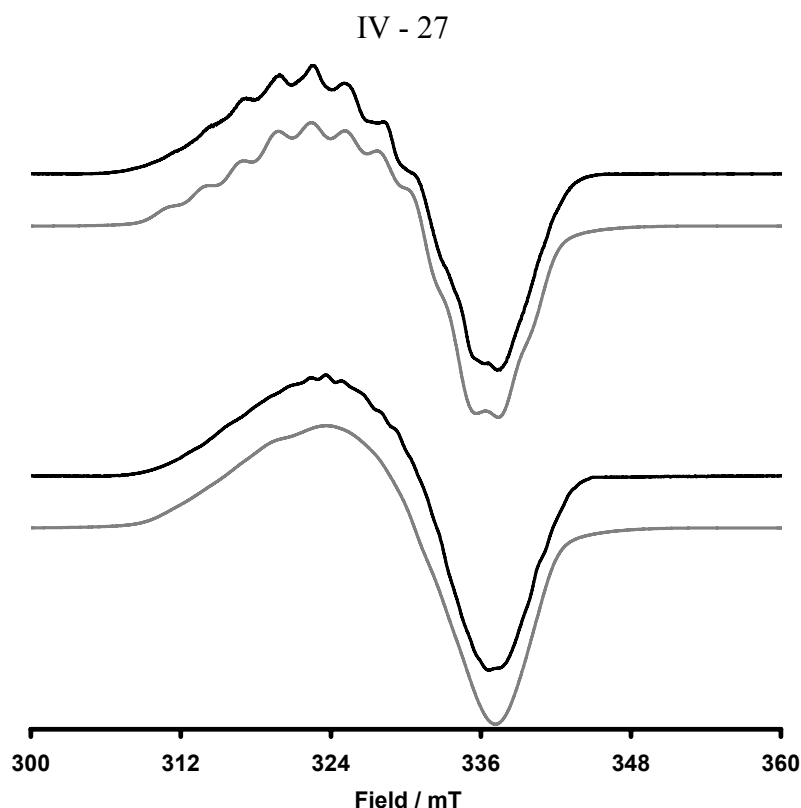


Figure IV.7: EPR spectrum (X-band) at 3.7 K. *Top:* **4.8** 2-Me-THF, experimental spectrum (black) and simulation (gray). *Bottom:* **4.10b** in 2-Me-THF, experimental spectrum (black) and simulation (gray).

EPR studies of **4.11** were conducted on the polycrystalline solid and the frozen dichloromethane:toluene (~20:1) glass. Both samples contained intense signals over the temperature range of 3.7-154 K. In both samples half-field absorptions were detected for the forbidden transition (165 mT) at 3.7 K confirming an S=1 state for **4.11** (Figure IV.8). The easily resolvable signal for the integer spin systems at X-band frequency must correspond to a system with very small zero-field splitting ($D < 0.3 \text{ cm}^{-1}$) of the triplet state. The spectrum of **4.11** in frozen dichloromethane:toluene glass (Figure IV.8, bottom) exhibits a broad, nearly axial signal consistent with a paramagnetic metal center. The very weak half-field signal is evident at 165 mT ($g = 4.02$) which is >1000 times smaller in amplitude than the major absorption feature at $g = 1.998$. The temperature dependence of the sample in a frozen dichloromethane glass was examined. The

integration of the microwave absorption at constant power (20 μW) was found to increase exponentially with decreasing temperature over the range 3.7–154 K which is characteristic of a ground state paramagnet. X-band EPR studies of a polycrystalline-powder sample over a temperature range of 3.7-100 K exhibited an axial signal at $g = 2.006$ with very weak half-field signal at 167 mT ($g = 4.020$) (Figure IV.8, top). No resolvable EPR signals characteristic of mononuclear Cu^{II} were evident in these studies.³⁸

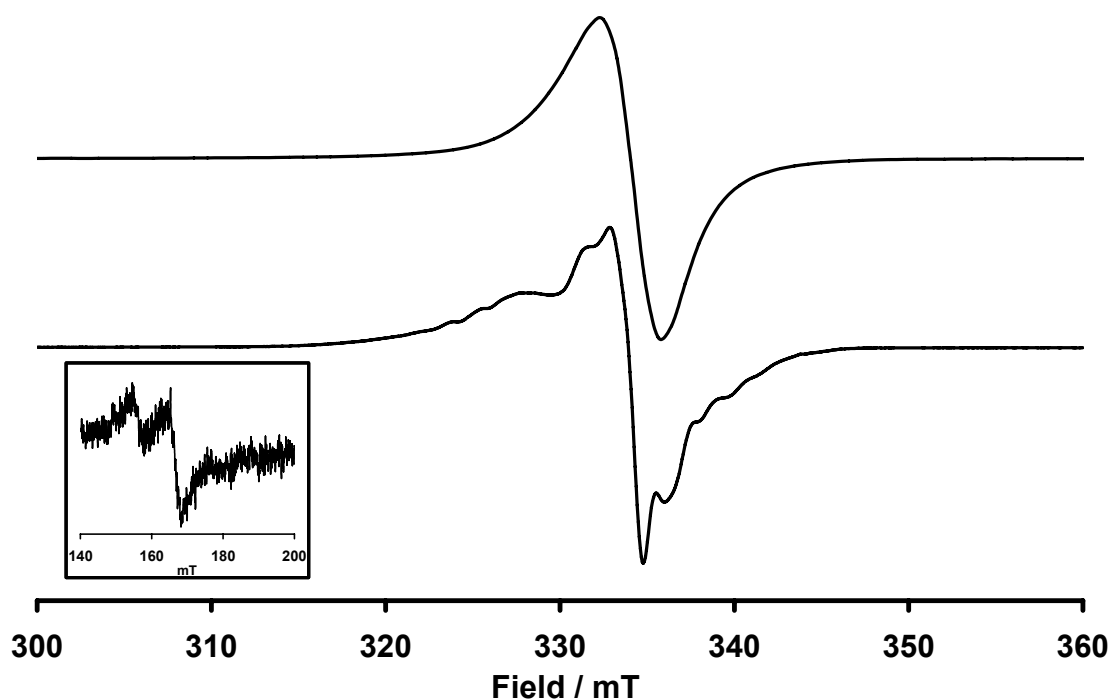


Figure IV.8: EPR spectrum (X-band). *Top:* polycrystalline solid sample of **4.11** (9.378 GHz, 6.377 μW). *Bottom:* frozen glass **4.11** in CH_2Cl_2 / toluene (9.339 GHz, 6.377 μW). *Bottom inset:* weak half-field signal in frozen glass (9.373 GHz, 6.393 mW).

Magnetic susceptibility studies of **4.10b** and **4.11** were conducted in an effort to better understand the electronic structure of these two dimers. For complex **4.10b**, fitting of χT as a function of T was achieved using the spin-only formula derived from the Curie law with an added term for the temperature independent paramagnetism (χ_{TIP}) using values of $g = 1.851(3)$ and $\chi_{\text{TIP}} = 0.001960(8)$ (eq. IV.1).

$$\chi T = (Ng^2\beta^2 / 4k) + \chi_{\text{TIP}} \cdot T \quad (\text{IV.1})$$

The relatively large value for the χ_{TIP} ³⁹ may be attributable to population of low-lying excited states as has been previously reported by Vila and Gray in their studies of the mixed-valent, Cu_A site of CcO.⁴⁰ From this data, **4.10b** was determined to have a μ_{eff} value which slopes linearly from 1.58-2.17 Bohr magnetons (BM) (3 K – 300 K) consistent with the expected doublet ground state of the cation. A value of 1.63 BM was determined for the room-temperature solution magnetic moment of **4.10b** in dichloromethane by the method of Evans⁴¹ and corresponds reasonably well with the values determined by SQUID magnetometry on the solid state material.

The magnet susceptibility of **4.11** was also probed by SQUID magnetometry and as was found by EPR the magnitude of χ_m increased exponentially with decreasing temperature as would be expected for a ground state triplet (Figure IV.9). Plotting of $\chi_m T$ as a function of T reveals a linear relationship where the value of $\chi_m T$ slopes from a minimum of 0.29 emu·T·mol⁻¹ at 3K to 0.447 at 300 K emu·T·mol⁻¹. From this data, values of μ_{eff} can be calculated and were found to increase steadily from 1.52 BM at 3 K to 1.90 BM at 300 K indicating an increasing effective magnetic moment with increasing temperature. Though the magnetic susceptibility would seem wholly consistent with **4.11** being a simple doublet spin system, analogous to **4.10b**, the elemental analysis of the SQUID sample indicates that two [SbF₆]⁻ anions must be present, which indicates the two-fold oxidation of **4.5**. Moreover, the susceptibility data is consistent with a single localized paramagnetic center and is likely not reflective of a system containing two exchange-coupled doublets as is classically observed for formal dicopper(II,II) complexes. The solution magnetic moment was also determined in this case by the

Evans' Method and afforded a value for the room temperature moment of $\mu_{\text{eff}} = 1.69 \text{ BM}$ in dichloromethane.

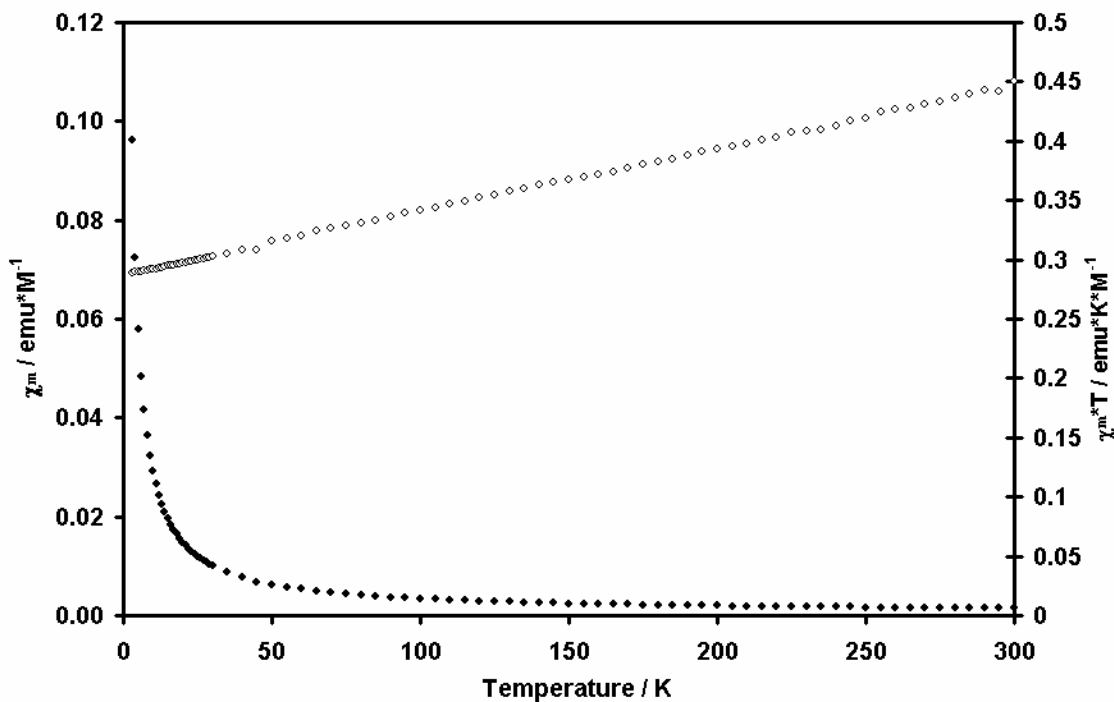


Figure IV.9: Magnetic susceptibility study of **4.11**. (●) χ vs. T; (○) χT vs. T

Absorption spectroscopy of the oxidized species. The absorption spectra for mixed valence complexes **4.8** and **4.10b** are shown in Figure IV.10. Both spectra are rich in electronic transitions which potentially derive from metal→ligand, ligand→metal, d→d, and intervalence charge transfer (IVCT) processes resulting from a vacancy in the singly occupied molecular orbital (SOMO). Gaussian fitting of the spectra affords values which are illustrative of the close relationship of the electronic structures of **4.8** and **4.10b** (Table IV.3). The same transitions are observed for each complex varying only slightly in the energy of the transition. Notably the intervalence charge transfer bands (IVCT) are easily recognizable from the spectra with $\lambda_{\text{max}} = 6068 \text{ cm}^{-1}$ and 5687 cm^{-1} for **4.8** and **4.10b**, respectively. This IVCT absorption band is characteristic of the delocalized

mixed-valence state of diatomically bridged $\text{Cu}^{1.5}\text{Cu}^{1.5}$ systems. The absorption with $\lambda_{\text{max}} = 31\,700\text{ cm}^{-1}$ and shoulder at $\sim 26\,500\text{ cm}^{-1}$ results from ligand centered $\pi \rightarrow \pi^*$ transitions which are perturbed to lower energy as a result of coordination to copper which is evident by comparison to the absorption spectra of d^{10} complexes **4.3**, **4.5**, and **4.6**.

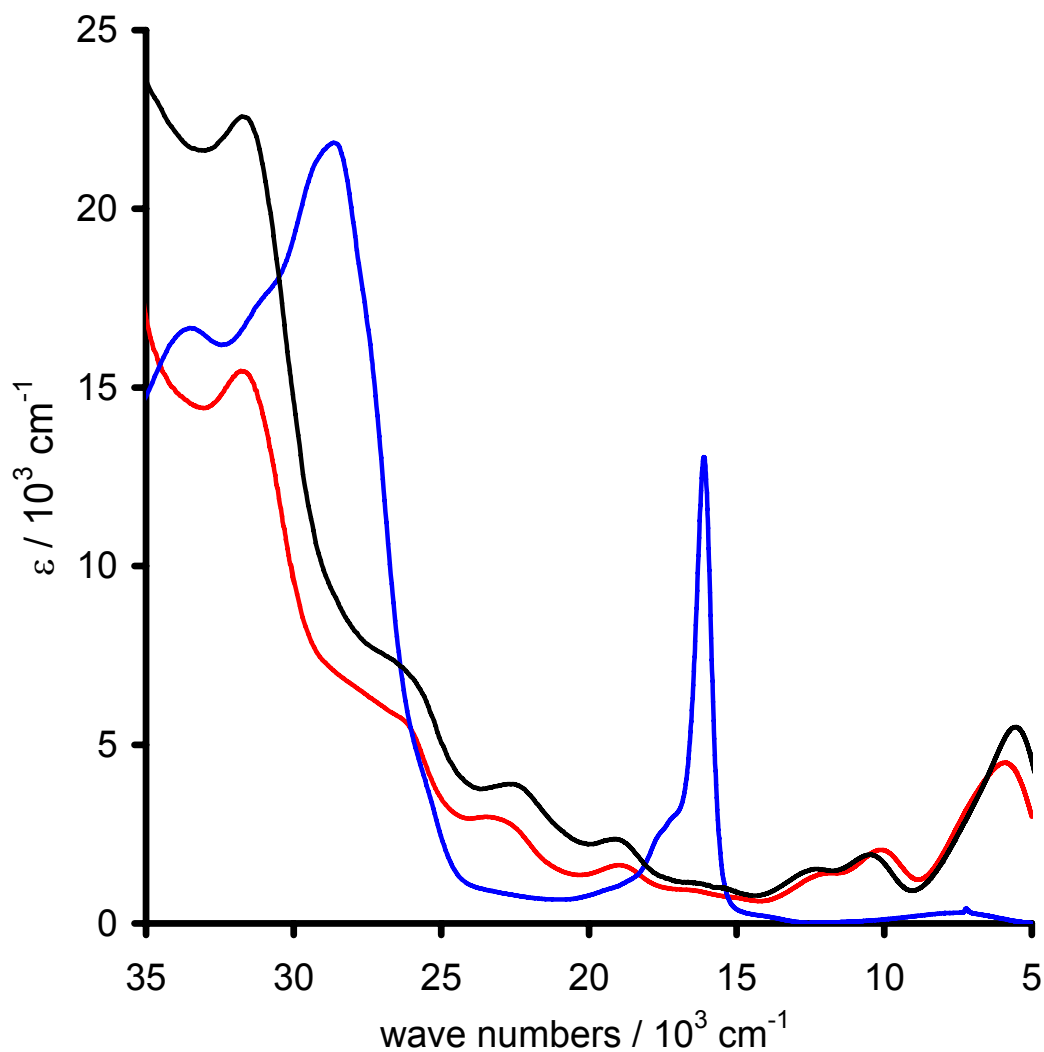


Figure IV.10: Absorption Spectra of **4.8** (red), **4.10b** (black), and **4.11** (blue) in CD_2Cl_2 .

The transitions #3 and #4 (Table IV.3) occur at higher energy in **4.8** than **4.10b**, but the trend reverses for transitions #5-#7. We speculate that transitions #3 and #4 result

from MLCT transitions by promoting an electron from the highest occupied orbitals to unoccupied ligand antibonding orbitals. Similarly, transitions #5-#7 could correspond to LMCT or d-d transitions from the lower filled orbitals to the SOMO. The intervalence charge transfer bands, #1 and #2, can be described in the same fashion, which is completely consistent the molecular geometries determined by X-ray crystallography. The longer Cu(1)-Cu(2) distance of **4.8** as compared to **4.10b** would obviously result in a diminished ability to exchange electrons in a direct Cu-Cu exchange regime and therefore should result in an increased energy of the charge transfer transition between valence states. This observation is also supportive of the proposed direct Cu-Cu interaction in the d^{10} complexes **4.3** and **4.5**.

Table IV.3: Absorption bands determined by Gaussian fitting of the spectra in Figure IV.10

#	4.8		4.10b		4.11	
	cm ⁻¹	ϵ (M ⁻¹ cm ⁻¹)	cm ⁻¹	ϵ (M ⁻¹ cm ⁻¹)	cm ⁻¹	ϵ (M ⁻¹ cm ⁻¹)
1	5516(15)	2248(242)	5327(2)	3180(93)	7782(22)	335(9)
2	6755(78)	2799(143)	6514(30)	2875(49)	16 105(1)	10 671(36)
3	10 065(14)	1416(25)	10381(7)	1232(12)	16 858(11)	2546(26)
4	12 012(27)	867(52)	12 337(14)	956(14)	18 522(51)	863(19)
5	16 152(70)	323(49)	16 062(23)	484(14)	28 184(10)	8953(229)
6	19 133(28)	967(47)	19 101(14)	1485(15)	30 082(61)	13 525(145)
7	22 831(13)	1595(55)	22 367(9)	2380(12)		
8	26 754(16)	2514(112)	26 115(8)	2885(23)		
9	31 403(5)	4986(64)	31 351(3)	5654(22)		

The spectra of the characteristically blue compound **4.11** is plotted in Figure IV.10 and exhibits similar charge transfer bands in the visible region between 21 000 and 13 000 cm⁻¹ as is observed in **4.10b**. Gaussian fitting of the spectra of **4.11** finds major visible transitions centered at 16 105(1) cm⁻¹ (10 671(35) M⁻¹cm⁻¹) and 16 858(11) cm⁻¹ (2546(26) M⁻¹cm⁻¹). The intensity of the absorption at 16105 and narrow line width (350 cm⁻¹) immediately suggests the possible presence of an organic or main group

radical cation in the system.⁴² A broad, low ϵ band is also present in the NIR position of the spectrum which is characteristic of a $d-d$ transition. This band assignment is suggested to be the transition from the highest energy filled d -orbital to the highest energy SOMO of **4.11**. Absorption bands corresponding to $d-d$ transition may also occur in complex **4.10b**; however, it is not distinguishable here because of the intense IVCT bands. Strong ligand-based absorptions at $28\,200\text{ cm}^{-1}$ with a shoulder at $\sim 26\,500\text{ cm}^{-1}$ are roughly consistent with the $\text{Cu}^{\text{I}}\text{Cu}^{\text{I}}$ complex, **4.5**, possibly suggesting that one of the Cu centers is closed shell. Further studies are needed in order to rigorously assign the visible bands to the appropriate ligand field transitions.

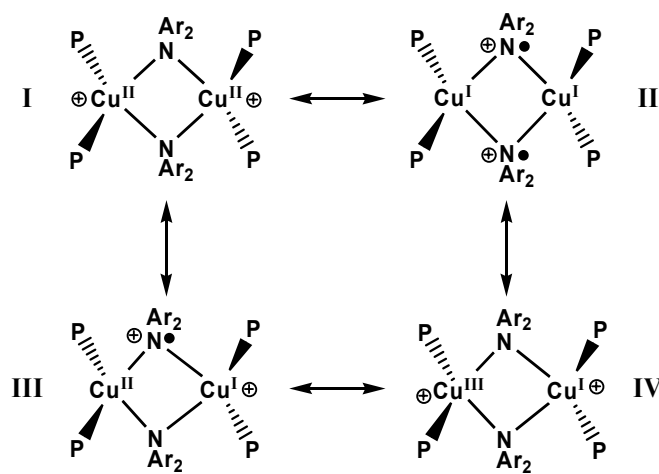


Figure IV.11: Possible resonance contributors to the electronic structure of **11** $\{\bullet\text{NAr}_2^+ = \text{delocalized, ligand center cation radical}\}$.

Discussion of the electronic localization in 4.11. Given the experimental data presented herein, four reasonable possibilities exist for the localized electronic structure of the dicationic dimer, **4.11**. The distinction of a “localized” electronic structure is made because in reality the cationic charge is delocalized across the entire molecular species, and the molecule is also likely to be resonance stabilized. From the electrochemical studies, an initial assignment of two Cu^{II} nuclei was postulated based on the assumption

of a symmetric, non-redox active ligand platform (Figure IV.11, I). In fact, the featureless cyclic voltammetry profile observed for the Zn dimer, **4.7**, in both THF and dichloromethane suggests the ligand is not redox active in the absence of Cu within the desired potential window. However the intense X-band EPR signal of **4.11**, which is indicative of a very small zero field splitting ($<0.3 \text{ cm}^{-1}$),⁴³ is not typical of dicopper(II,II) complexes with dinuclear bridging units.⁴⁴ The magnetic susceptibility data is not consistent with an exchange coupled triplet spin system. Exchange-coupling would have been expected in this case given the close molecular proximity of the two Cu^{II} nuclei. The plot of χT as a function of T was experimentally determined and can be crudely fit using the Bleany-Bowers exchanged coupled model (eq. IV.2) with values for $g = 1.238(1)$ $J = -0.028(26) \text{ cm}^{-1}$, and $\chi_{\text{TIP}} = 5.32(2) \times 10^{-4} \text{ emu} \cdot \text{mol}^{-1}$. However, given the large uncertainty in J, and the unreasonably low g value, the presented data would appear largely inconsistent with a simple $S=1$ exchange coupled model.

$$\chi T = (2N g^2 \beta^2 / k) \cdot [3 + e^{-J/kT}]^{-1} + \chi_{\text{TIP}} \cdot T \quad (\text{IV.2})$$

Upon inspection of the Cu_2N_2 core geometry of **4.11** afforded by X-ray crystallography, structural nonequivalence between the two copper sites is immediately apparent. This structural data then demands that electronic asymmetry must also exist in **4.11**, and so **I** can be eliminated from consideration as a major resonance contributor. For the same reason, **II** is also eliminated as a major contributor to the electronic structure ($\bullet\text{NAr}_2^+$ denotes a ligand centered cation radical which is not restricted to localization on the N atoms). If two ligand centered radicals were present in the structure, as shown in **II**, there would be no apparent need for nonequivalence between the copper centers.

Moreover, the radical character should also be manifest in the electrochemical studies of **4.6**.

Resonance contributors **III** and **IV**, however, are both consistent with the asymmetry observed for **4.11** by X-ray crystallography. The apparent dative Cu(1)-N interactions (~ 2.4 Å) are assigned to a formally cationic Cu^I center which is closed shell. The two shorter Cu(2)-N bond distances (~ 2.0 Å) are clearly covalent in nature and consistent with the bond lengths observed previously for copper amides. Based on this, an assignment of a neutral Cu^{II} (**III**) or a cationic Cu^{III} (**IV**) center are reasonable.

In order to balance the oxidation state of **III**, a delocalized cation radical must also be present in the ligand. Based on literature precedent for the disproportionation of $2 \text{Cu}^{\text{II}} \rightarrow \text{Cu}^{\text{I}} + \text{Cu}^{\text{III}}$, we speculate the **4.11** forms as a result of rapid intramolecular disproportionation of a dicopper(II,II) complex.⁴⁵ From the data presented in the current work, a conclusive assignment of whether **III** or **IV** is the dominant resonance contributor cannot be established. However this electronic structure problem is not new in the field of bioinorganic chemistry and has been addressed for many years in the studies of galactose oxidase and ribonucleotide reductase.⁴⁶ In these cases, conclusive assignments were only attained by the use of X-ray absorption near-edge structure (XANES) analysis.

Given the available data, the best description of the electronic structure of **4.11** is **IV**, though it is likely resonance stabilized through **III**. This formulation presents the opportunity to study a d^8 Cu^{III} (S=1) nucleus in a compressed tetrahedral environment, something that has not been previously characterized. Previously, S=1 Cu^{III} systems have been observed exclusively in octahedral geometries.^{47,48} Though pseudo-tetrahedral

examples of Cu^{III} have not been reported, a large volume of literature does exist for isoelectronic Ni^{II} complexes in distorted tetrahedral environments with $S=1$ ground states.⁴⁹ The formulation of **IV** is supported by the magnetic data. Though the EPR spectrum of **11** has not been effectively simulated, the experimental spectrum is reasonable for a system with two unpaired electrons localized on a single Cu center (spin $3/2$) with a small zero-field splitting parameter. Further, the lack of prominent ferromagnetic or antiferromagnetic exchange coupling from the SQUID data supports the postulate of spin localization.

The magnetic moment observed in both solid (SQUID) and solution (Evans' method) samples is significantly lower than the spin only value for two unpaired electron (2.8 BM), and is likely the result of considerable spin-orbit coupling or population of low-lying singlet excited states.^{50,51} The magnitude of 1.90 BM for $\mu_{\text{eff-300K}}$ of **4.11** seems more consistent with a doublet spin system than a triplet, and is remarkably similar to **4.10b**. The possibility of the SQUID sample in fact being **4.10b** and not **4.11** is not possible, because the EPR and optical spectroscopy of the sample used for the SQUID experiment were not characteristic of **4.11**, and showed no signs of degradation. Further, the microanalysis of the sample of **4.11** used for the SQUID is precisely consistent with the dicationic formulation of **4.11**, which along with the X-ray diffraction study definitively establishes the two electron oxidation of **4.5**. Subnormal magnetic moments have been observed previously for paramagnetic Cu^{III} . Weighardt and co-workers reported a high-spin, octahedral $\text{Cu}^{\text{III}}\text{S}_6$ complex which is reported to have a $\mu_{\text{eff}} = 2.4$ BM at 20 K.

IV.C. Summary and Future Directions

In this manuscript we have presented a molecular dicopper system which can stabilize multiple oxidation states with minimal structural reorganization and no additional ligand coordination to the Cu centers. The spectroscopic, magnetic, and redox studies described herein are indicative of the highly covalent Cu_2N_2 diamond core architecture of the presented metal complexes. An important aspect of this system is that the ligand superstructure remains externally rigid while allowing minor adjustments within the metal-ligand core to accommodate a variety of metals and oxidation states. We characterize this system as a demonstration of the “entatic state” which is embodied by the polymetallic cofactors that mediate multi-electron redox processes at or near enzymatic functional sites. Particularly, this manuscript details the synthesis and study of dicopper complexes (**4.3** and **4.5**) which exhibit highly efficient luminescence and can sustain two reversible one electron oxidations $\{4.5 \rightarrow 4.10 \rightarrow 4.11\}$. Unique to this dicopper system is that each of these oxidized species can be isolated and structurally characterized, and so we are able to observe that there is minimal structural reorganization of the molecule and no change to the metal coordination number. The unexpected assignment of a putative pseudo-tetrahedral $\text{Cu}^{\text{III}}/\text{Cu}^{\text{I}}$ dimer further serves to illustrate the varied electronic states which the ligand can support. The covalent nature of the system is also evident in the exceptionally high quantum yields and long emission lifetimes which are observed for the dicopper systems, but not for the Zn_2N_2 (**4.6**) or CuZnN_2 (**4.7**) complexes. In this manuscript, we also present one of the few systems where the one-electron oxidation products of a highly luminescent copper complex (**4.8** and **4.10**) can be isolated and are structurally unperturbed. This presents an ideal opportunity for the acquisition and

comparison of an excited-state molecular structure to *both* the ground-state of the luminophore and the one-electron oxidized complex. The analogous dizinc and heterobimetallic copper-zinc molecular complexes were also been prepared and aided in the understanding of the spectroscopic and redox characteristics of **4.5**.

Future work involving this molecular system will address the electronic structure assignment of **4.11** and potential analogs. The utilization of more advanced spectroscopic methods coupled with appropriate theoretical studies will allow for a more accurate description of the electronic distribution of **4.11**. Previously, XANES, XMCD, and resonance Raman techniques have been utilized to deconvolute similar electronic structure problems and will be pursued in due course. We also intend to address the excited state reactivity of **4.3** and **4.5**. Previously, we have reported the time-resolved diffusion-limited emission quenching of **4.3** by 2,6-dichloroquinone. In preliminary studies, we have found the intriguing result that by saturating a THF solution of **4.5** with N₂O, 97% of the emission is quenched. Prolonged irradiation of **4.5** under N₂O with visible light (> 375 nm) results in total consumption of the starting material **4.5**, and a mixture of undetermined products. Reaction in the absence of light was not observed. Regardless of the product composition this is the first reported example of a molecular copper complex showing any such activity with N₂O which presumably is facilitated by the highly reducing excited state of **4.5**. These results are particularly interesting in the context of understanding the mechanism of the tetranuclear Cu₄ functional site in N₂OR and it is our hope that direct evidence for the intermediacy Cu-[NNO] adducts in this decomposition will be attainable.

IV.D. Experimental Section

General. All manipulations were carried out using standard Schlenk or glove-box techniques under a dinitrogen atmosphere. Unless otherwise noted, solvents were deoxygenated and dried by thorough sparging with N₂ gas followed by passage through an activated alumina column. Non-halogenated solvents were tested with a standard purple solution of sodium benzophenone ketyl in tetrahydrofuran to confirm effective oxygen and moisture removal. All reagents were purchased from commercial vendors and used without further purification unless otherwise stated. Mesityl copper, 2, 2'-difluorodiphenylamine, diethylphosphoramidous dichloride,⁵² 4,4'-di-*t*-butyldiphenylamine,⁵³ and [Cp₂Fe][B(C₆H₃(CF₃)₂)₄]⁵⁴ were prepared according to literature procedures. Elemental analyses were performed by Desert Analytics, Tucson, AZ. Deuterated solvents were purchased from Cambridge Isotope Laboratories, Inc. and degassed and dried over activated 3 Å molecular sieves prior to use. A Varian Mercury-300 or INOVA-500 NMR spectrometer was used to record ¹H, ¹³C, ¹⁹F and ³¹P NMR spectra at ambient temperature. ¹H chemical shifts were referenced to residual solvent. GC-MS data was obtained by injecting a dichloromethane solution into an Agilent 6890 GC equipped with an Agilent 5973 mass selective detector (EI). High-resolution EI mass spectroscopy was carried out by the Caltech Chemistry Mass Spectral Facility using a JEOL JMS600. UV-vis measurements were taken on a Cary 500 UV/Vis/NIR Spectrophotometer or a Cary 50 UV/Vis Spectrophotometer using a 1.0 cm or a 0.1 cm quartz cell with a Teflon stopper. X-ray diffraction studies were carried out in the Beckman Institute Crystallographic Facility on a Bruker Smart 1000 CCD diffractometer.

Magnetic Measurements. Measurements were recorded using a Quantum Designs SQUID magnetometer running MPMSR2 software (Magnetic Property Measurement System Revision 2). Data were recorded at 5000 G. Samples were suspended in the magnetometer in a clear plastic straw sealed under nitrogen with Lilly No. 4 gel caps. Loaded samples were centered within the magnetometer using the DC centering scan at 35 K and 5000 G. Data were acquired at 3–30 K (one data point every 1 K) and 30–300 K (one data point every 5 K). The magnetic susceptibility was adjusted for diamagnetic contributions using the constitutive corrections of Pascal's constants.⁵⁵ The molar magnetic susceptibility (χ_m) was calculated by converting the calculated magnetic susceptibility (χ) obtained from the magnetometer to a molar susceptibility (using the multiplication factor $\{(\text{molecular weight})/[(\text{sample weight}) * (\text{field strength})]\}$). Curie-Weiss behavior was verified by a plot of χ_m^{-1} versus T. Effective magnetic moments were calculated using equation IV.3. Solution magnetic moments were measured by the Evans method.

$$\mu_{\text{eff}} = \text{sqrt}(7.997 \chi_m T) \quad (\text{IV.3})$$

EPR Measurements. X-band EPR spectra were obtained on a Bruker EMX spectrometer (controlled by Bruker Win EPR Software v. 3.0) equipped with a rectangular cavity working in the TE₁₀₂ mode. Variable temperature measurements were conducted with an Oxford continuous-flow helium cryostat (temperature range 3.6–300 K). Accurate frequency values were provided by a frequency counter built into the microwave bridge. Solution spectra were acquired in 2-methyltetrahydrofuran or 20:1 dichloromethane:toluene solution. Sample preparation was performed under a dinitrogen atmosphere in an EPR tube equipped with a ground glass joint.

Electrochemistry. Electrochemical measurements were carried out in a glove-box under a dinitrogen atmosphere in a one-compartment cell using a BAS model 100/W electrochemical analyzer. A platinum electrode and platinum wire were used as the working and auxiliary electrodes, respectively. The reference electrode was Ag/AgNO₃ in THF or CH₂Cl₂. Solutions of electrolyte (0.35 M tetra-*n*-butylammonium hexafluorophosphate in THF or 0.1 M tetra-*n*-butylammonium hexafluorophosphate in CH₂Cl₂) and analyte were prepared in a glove-box.

Lifetime measurements. A solution of analyte in either tetrahydrofuran or dichloromethane was prepared in a nitrogen filled glovebox. The quartz cuvettes (1 cm pathlength) were charged with this solution, sparged briefly with argon, and sealed with a ground-glass stopper. The absorption spectra were acquired both before and after measurements to ensure the sample was not photodegrading. Luminescence lifetime measurements were carried out using one of the configurations listed below (A-C) below and specified in Table IV.4.

Configuration A. Fluorescence decay kinetics measurements were carried out as previously described⁵⁶ using 8 ns pulses (at a repetition rate of 10 Hz) from a Nd:YAG laser pumped OPO (Quanta Ray Pro, Spectra Physics). The luminescence was dispersed through a monochromator (Instruments SA DH-10) onto a photomultiplier tube (PMT) (Hamamatsu R928). The PMT current was amplified and recorded with a transient digitizer (Tektronix). Measurements were performed with $\lambda_{\text{ex}} = 460$, $\lambda_{\text{em}} = 510$ nm at 298 K. A 500 nm low-pass filter was placed in front of the PMT in order to eliminate noise due to scattered laser light. The emission decay was averaged over 50 laser pulses and fit to an exponential function from which k_{obs} was determined.

Configuration B. Fluorescence decay kinetics measurements were carried out as previously described⁵⁷ using the third harmonic of a regeneratively amplified, mode-locked Nd:YAG laser (355 nm) for excitation, and a picosecond streak camera (C5680, Hamamatsu Photonics, Hamamatsu City, Japan) for detection. The fluorescence was selected with both long- and short-pass cutoff filters ($450 \text{ nm} < \lambda_{\text{obs}} < 500 \text{ nm}$, **7**; $400 \text{ nm} < \lambda_{\text{obs}} < 450 \text{ nm}$; **6a**).

Configuration C. Fluorescence decay kinetics measurements were carried out as previously described⁵⁸ using the second harmonic (435 nm) of a regeneratively amplified femtosecond Ti:sapphire laser (Spectra-Physics) as an excitation source, and a picosecond streak camera (C5680, Hamamatsu Photonics, Hamamatsu City, Japan) in the photon-counting mode for detection. Emission was selected by an interference filter ($\lambda = 488 \pm 5 \text{ nm}$).

Table IV.4: Data for Excited State Lifetime Measurements.

Solution	Config.	$k_{\text{obs}} \text{ (s}^{-1}\text{)}$	Lifetime (τ , $1/k_{\text{obs}}$) (μs)
150 μM 4.2 in pet. ether	C	k_1 (75%) 3.74E08	τ_1 2.7E-03
		k_2 (25%) 1.25E08	τ_2 8.0E-03
10 μM 4.3 in THF	–	9.14E+04 ^a	10.9 ^a
10 μM 4.5 in THF	A	8.72E+04	11.4
10 μM 4.6 in CH ₂ Cl ₂	B	–	–
10 μM 4.7 in CH ₂ Cl ₂	B	$\geq 2\text{E}+09$	$\leq 5\text{E}-04$

(a) Value taken from: Harkins, S. B.; Peters, J. C. *J. Am. Chem. Soc.* **2005**, *127*, 2030.

Quantum yield experiments. Emission spectra were recorded on a Spex Fluorolog-2 spectro-fluorometer. A solution of analyte or reference in either benzene or tetrahydrofuran was prepared in a nitrogen filled glovebox. Cuvettes (1 cm path) were charged with this solution, sparged briefly with argon, and sealed with a greased ground-glass stopper. The absorption spectra were acquired both before and after fluorescence

measurements to ensure the sample was not degrading. Fluorescent measurements were performed at the specified wavelength and corrected for detector response after equilibration to 298 K. The area under the curve of the emission spectrum was determined using standard trapezoidal integration methods. Quantum yields (Table IV.5) were then calculated by the methods described by Demas and Crosby⁵⁹ using eqn. IV.4 .

$$Q = (Q_R)(I / I_R)(OD_R / OD) (n^2 / n_R^2) \quad (\text{IV.4})$$

- Q: quantum yield of the sample.
 Q_R: quantum yield of reference.
 I: integrated intensity of analyte.
 I_R: integrated intensity of reference.
 OD_R: optical density of the reference in absorption units.
 OD: optical density of the analyte in absorption units.
 n: index of refraction of the solvent in which the analyte was dissolved.
 n_R: index of refraction of the solvent in which the reference was dissolved.

Table IV.5: Data for Quantum Yield Measurements.

Solution	λ_{ex}	OD (meas.)	I (meas.)	Q (cacl.)
Quantum Yield of 4.2				
30 μM 4.3 in benzene	340 nm	0.819	2.048E09	0.68 ^a
50 μM 4.2 in benzene	340 nm	1.021	2.184E09	0.58
Quantum Yield of 4.5				
10 μM 4.3 in THF	440 nm	3.807E-02	6.547E08	0.68 ^a
8.2 μM 4.5 in THF	440 nm	3.786E-02	5.504E08	0.57
Quantum Yield of 4.7				
C ₂₀ H ₂₄ N ₂ O ₂ in 1.0 N H ₂ SO ₄ ^{b,c}	370 nm	0.2742	4.237E09	0.55
72 μM 4.7 in CH ₂ Cl ₂	370 nm	0.2703	5.073E06	7.47E-04
N₂O Experiment quenching				
8.2 μM 4.5 in THF / no N ₂ O	440 nm	4.008E-02	5.091E08	0.68 ^a
8.2 μM 4.5 in THF / sat. N ₂ O	440 nm	3.924E-02	1.611E07	0.022

(a) Value taken from: Harkins, S. B.; Peters, J. C. *J. Am. Chem. Soc.* **2005**, *127*, 2030. (b) C₂₀H₂₄N₂O₂ = quinine. (c) Ref. 59.

Synthesis of Lithium Diisobutylphosphide. In a 500 mL Erlenmeyer flask diisobutylphosphine (25.0 g, 0.171 mol) was dissolved in 200 mL of petroleum ether and cooled to -80 °C, at which time at 1.6 M solution of ⁿbutyl lithium in hexane (107 mL,

0.171 mol) was added over 20 min. The reaction was then stirred at ambient temperature for 24 h, concentrated in vacuo to ca. 50 mL, and the white solids were then collected on a sintered-glass frit. Washing of the solids with petroleum ether afforded a single phosphorous containing product (21.1 g, 81%) by ^{31}P NMR upon drying.

$^{31}\text{P}\{^1\text{H}\}$ NMR (121.5 MHz, THF): -91.2.

Synthesis of Bis(2-(diisobutylphosphino)phenyl)amine, (PNP)H (4.1). In a 250 mL sealable reaction bomb, a 1.6 M *n*-butyl lithium solution (7.90 mL, 12.6 mmol) in hexanes was added dropwise to a solution of bis(2-fluorophenyl)amine (2.46 g, 12.0 mmol) in THF (20 mL). After stirring for 15 min, the solution was concentrated in vacuo to remove the majority of the reaction volatiles. A solution of lithium diisobutylphosphide (5.47 g, 36 mmol) in THF (40 mL) was then added and the vessel was sealed with a Teflon plug. The reaction was heated at 45 °C for 4 days and was monitored by $^{19}\text{F}\{^1\text{H}\}$ NMR to confirm the complete disappearance of the aryl fluoride resonance. The reaction was then quenched with methanol (5 mL) and the solution became yellow in color. Petroleum ether (50 mL) was added and the mixture was filtered twice through Celite to remove solids. Removal of the solvent in vacuo afforded an orange oil which was diluted in petroleum ether (30 mL) and filtered through two plugs of silica in a 60 mL sintered-glass frit. Evaporation of the solvent under reduced pressure afforded a spectroscopically pure, pale green oil (4.10 g, 75%).

^1H NMR (300.1 MHz, CDCl_3): δ 8.03 (t, 1H), 7.52 (m, 2H), 7.33 (m, 2H), 7.26 (t, 2H), 7.00 (t, 2H), 1.73 (m, 12H), 1.08 (d, 12), 1.03 (d, 12H). $^{13}\text{C}\{^1\text{H}\}$ NMR (75.5 MHz, CDCl_3): δ 147.8, 131.8, 129.4, 128.0, 121.0, 119.3, 116.7, 39.4, 26.6, 24.7, 24.3. $^{31}\text{P}\{^1\text{H}\}$ NMR (121.5 MHz, CDCl_3): δ -54.5. UV-vis (benzene, $\text{nm}(\text{M}^{-1}\text{cm}^{-1})$): 302(18,700), 334

sh. FAB+ MS: Calcd. for $C_{28}H_{45}NP_2$: 457.3027. Found: 458.3122 [M+H], 400.2226 [M-^tBu], 312.1904 [M-(^tBu₂P)].

Synthesis of {(PNP)Li}₂ (4.2): At ambient temperature a 1.6 M ⁿbutyl lithium solution (4.0 mL, 6.4 mmol) in hexanes was added dropwise to a solution of **4.1** (2.63 g, 5.76 mmol) in petroleum ether (50 mL) over 15 min. The reaction was stirred for 30 min, at which time a solid began to precipitate. The solution was concentrated to ca. 30 mL and cooled to -30 °C for 12 h. The resulting solids were collected on a sintered-glass frit as a fine pale yellow powder and dried thoroughly (2.24 g, 84 %). Crystals suitable for X-ray diffraction were obtained by cooling a concentrated solution of **4.2** in petroleum ether to -35 °C.

¹H NMR (499.9 MHz, C₆D₆): δ 7.21 (m, 2 H), 7.06 (m, 4 H), 6.71 (m, 2 H), 1.8-0.6 (br m, 36 H). ¹³C{¹H} NMR (125.7 MHz, C₆D₆): δ 170.6, 132.4, 131.2, 128.7, 128.1, 118.6, 42.3, 36.2, 26.3, 25.3. ³¹P{¹H} NMR (121.5 MHz, C₆D₆): δ -49.4 (q, 61 Hz). UV-vis (benzene, nm(M⁻¹cm⁻¹)): 303(18,200), 359(17200), 398 sh, 414 sh. Anal. calcd. for C₅₆H₈₈Li₂N₂P₄: C, 72.55; H, 9.57; N, 3.02. Found: C, 73.21; H, 9.43; N, 3.14.

Synthesis of {(PNP)Cu}₂ (4.3): A solution of **4.2** (1.00 g, 2.16 mmol) in diethyl ether (20 mL) was added to a slurry of CuBr·S(CH₃)₂ (0.466 g, 2.27 mmol) in diethyl ether (30 mL) and stirred for 12 h. The solvent was removed in vacuo and the resulting yellow solids were dissolved in petroleum ether (50 ml) and filtered to remove insoluble materials. Removal of petroleum ether and drying the yellow solids in vacuo afforded analytically pure material (1.04 g, 92%). Crystals suitable for X-ray diffraction were obtained by slow-evaporation of a petroleum ether solution of **4.3**.

^1H NMR (499.9 MHz, CD_2Cl_2): δ 7.20 (m, 4H), 6.93 (m, 4H), 6.71 (br d, 4H), 6.61 (t, 4H), 1.81 (m, 4H), 1.58 (m, 8H), 1.39 (m, 8H), 1.29 (m, 4H), 0.99 (d, 12H), 0.73 (d, 12H), 0.70 (d, 12H), 0.60 (d, 12H). $^{13}\text{C}\{^1\text{H}\}$ NMR (125.7 MHz, CD_2Cl_2): δ 169.4, 131.8, 130.5, 128.7, 125.2, 117.8, 40.2, 36.4, 26.3, 26.2, 26.0, 25.7, 25.4, 25.1. $^{31}\text{P}\{^1\text{H}\}$ NMR (121.5 MHz, C_6D_6): δ -33.9. UV-vis (THF, $\text{nm}(\text{M}^{-1}\text{cm}^{-1})$): 294 (sh), 311 (17000), 350 (42,000), 387 sh, 423 (4400), 446 sh. Anal. calcd. for $\text{C}_{56}\text{H}_{88}\text{Cu}_2\text{N}_2\text{P}_4$: C, 64.65; H, 8.53; N, 2.69. Found: C, 64.54; H, 8.25; N, 2.62.

Synthesis of diisobutylchlorophosphine: Neat diethylphosphoramidous dichloride (58.0 g, 0.333 moles) was added to a 2.0 M solution of isobutyl magnesium chloride in diethyl ether (350 mL) at 0 °C over a period of 30 min. Following addition, the solution was stirred at ambient temperature for 1 h and the crude ^{31}P NMR indicated that the starting material had been consumed and diisobutylchlorophosphine (^{31}P NMR: 47.9 ppm, $(\text{Et})_2\text{NP}(\text{iBu})_2$) was the only phosphorus containing product. The solution was again cooled to 0 °C and a 2.0 M solution of anhydrous HCl in ether (350 mL) was added via cannula while stirring vigorously. A considerable amount of solid precipitated over a 2 h period and the supernatant was isolated by cannula filtration. The solids were extracted with 200 mL of diethyl ether, and the solvent was removed by fractional distillation. The crude viscous oil was purified by fractional vacuum distillation (26–29 °C at 0.005 Torr) followed by removal of the residual diethyl ether by prolonged exposure to vacuum at -10 °C with stirring. The product was isolated as a spectroscopically pure, colorless oil (38.6 g, 65 %) which exhibited a single resonance by ^{31}P NMR spectroscopy consistent with previously published results.⁶⁰

^1H NMR (300 MHz, C_6D_6): δ 1.87 (m, 2H), 1.78 (br m, 2H), 1.24 (br m, 2H), 0.90 (br s, 12H). $^{31}\text{P}\{^1\text{H}\}$ NMR (121 MHz, C_6D_6): δ 109.9.

Synthesis of di(2-bromo-4-*t*-butylphenyl)amine: In air, neat Br_2 (3.6 mL, 0.071 mol.) at ~ 5 °C was added dropwise to a slurry of 4,4'-di-*t*-butylphenylamine (10.0 g, 0.0356 mol) in acetic acid at ~ 16 °C. Following addition, the solution was stirred at ambient temperature for 2 hours and a dilute solution of $\text{Na}_2\text{S}_2\text{O}_4$ (500 mL) was added and the resulting solution was stirred for 15 min. The solids were collected on a frit and washed with H_2O (3 x 200 mL). The crude product was purified by crystallization at -20 °C from methanol/chloroform as a white solid (12.35 g, 80 %).

^1H NMR (300 MHz, CDCl_3): δ 7.59 (m, 2H), 7.23 (m, 4H), 6.30 (br s, 1H) 1.32 (s, 18H). $^{13}\text{C}\{^1\text{H}\}$ NMR (75.5 MHz, CDCl_3): 145.9, 137.9, 130.2, 125.3, 117.8, 114.1, 34.5, 31.5. GC-MS(ES) 439 (M), 424 (M- CH_3).

Synthesis of bis(2-diisobutylphosphino-4-*t*-butylphenyl)amine, (*t*-Bu₂-PNP)H (4.4): A 1.6 M solution of *n*-butyl lithium in hexane (26 mL) was added dropwise to a solution of di(2-bromo-4-*t*-butylphenyl)amine (6.0 g, 13.7 mmol) in diethyl ether (100 mL) at -70 °C with stirring. The solution immediately became yellow in color and was stirred at ambient temperature for 4 h at which time a precipitate had formed. The reaction mixture was again cooled to -70 °C, at which time diisobutylchlorophosphine (7.67 g, 41.7 mmol) was added as a 1:1 solution with diethyl ether and the reaction was allowed to warm to room temperature. After 36 hours at ambient temperature a large amount of precipitate had formed, and was removed by filtration through Celite[®] after diluting the reaction solution with diethyl ether (100 mL). The filtrate was treated with a 1.0 M solution of anhydrous HCl in ether (2 x 50 mL) which immediately resulted in the precipitation of

the product as an HCl salt. The solids were collected on a frit and washed with petroleum ether (3 x 50 mL). These solids were suspended in a 4:1 mixture of THF:CH₃CN and excess (> 4 equiv.) NaOMe was added and the mixture was stirred for 2 h. The solvent was removed in vacuo. The sticky solids were extracted with petroleum ether (50 mL) and filtered through Celite[®]. The solvent was removed from the filtrate under reduced pressure. The resultant tacky translucent solid was stirred in CH₃CN for 1 h, affording a tractable white solid (5.35 g, 68%) which was pure by NMR spectroscopy.

¹H NMR (300 MHz, CD₂Cl₂): δ 7.66 (t, 1H), 7.46 (m, 2H), 7.16 (m, 4H), 1.34 (s, 18H), 1.00 (d, 6H), 0.94 (d, 6H). ¹³C{¹H} NMR (75.5 MHz, CD₂Cl₂): δ 145.9, 143.5, 128.8, 127.4, 126.7, 116.6, 39.6, 34.9, 31.9, 27.1, 24.9, 24.6. ³¹P{¹H} NMR (121 MHz, CD₂Cl₂): δ -53.1. Anal. calcd. for C₃₆H₆₁NP₂: C, 75.88; H, 10.79; N, 2.46; Found: C, 75.35; H, 10.20; N, 2.81. UV-vis (THF, nm(M⁻¹cm⁻¹)): 303 (20700), 344 sh.

Synthesis of {(^tBu₂-PNP)Cu}₂ (4.5): Mesityl-Cu (128 mg, 0.702 mmol) and **4.4** (400 mg, 0.702 mmol) were dissolved in petroleum ether and stirred for 12 hr at ambient temperature. The emissive yellow solution was filtered through a glass micro-filter and the solvent was in vacuo. The bright yellow solid was stirred in CH₃CN for 1 h in the dark and collected on a frit. Drying of the solids *in vacuo* afforded a finely divided analytically pure yellow solid (400 mg, 90%). Crystals suitable for X-ray diffraction were obtained by slow evaporation of the solvent from a solution of **4.5** in THF.

¹H NMR (300 MHz, C₆D₆): δ 7.43 (m, 4H), 7.02 (m, 8H), 2.12 (n, 8H), 1.84 - 1.50 (m, 16H) 1.34 (s, 36H), 1.15 (d, 12), 0.89 (dd, 24), 0.76 (d, 12H). ¹³C{¹H} NMR (75.5 MHz, C₆D₆): δ 168.1, 139.5, 128.5, 128.2, 127.1, 125.4, 40.0, 36.3, 34.6, 32.3, 26.7, 26.5, 25.9, 25.8. ³¹P{¹H} NMR (121 MHz, C₆D₆): δ -35.3. Anal. calcd. for C₇₂H₁₂₀Cu₂N₂P₄: C,

68.38; H, 9.56; N, 2.21; Found: C, 68.55; H, 9.38; N, 2.61. UV-vis (THF, nm(M⁻¹cm⁻¹)): 295 (20 500), 318 (21 100), 357 (33 300), 383 sh, 433 (4600), 459 (3800).

Synthesis of [(^tBu₂-PNP)Zn]₂][PF₆]₂ (4.6a): In a 20 mL reaction vial, a 2.0 M solution of CH₃ZnCl in THF (68.0 mg, 0.132 mmol) was added to a solution of **4.4** (75 mg, 0.13 mmol) in THF (5 mL). The solution was heated to 75 °C for 4 h. TIPF₆ (46.1 mg, 0.132 mmol) was added and the solution was heated for 12 h longer. The solvent was removed *in vacuo* and the resultant solids were washed with petroleum ether (2 x 5 mL). The solids were then extracted into 1:1 dichloromethane:THF (2 mL) and layered with petroleum ether (10 mL) which afforded analytically pure, colorless crystals (59 mg, 57%) after 2 days.

¹H NMR (300 MHz, CD₂Cl₂): δ 7.62 (m, 4H), 7.55 (dd, 4H), 6.68 (td, 4H), 2.27 (m, 4H), 2.05(m, 4H), 1.9–1.4 (m, 16H), 1.36 (s, 36H), 1.06 (d, 12H), 0.91 (d, 12H), 0.83 (d, 12H), 0.75 (d, 12H). ¹³C{¹H} NMR (125.6 MHz, CD₂Cl₂): δ 160.2, 149.2, 133.3, 130.1, 127.6, 116.0, 35.3, 33.5, 32.6, 31.5, 25.5–24.2 (m, -CH₃). ³¹P{¹H} NMR (121 MHz, CD₂Cl₂): δ -36.6 (s), -143.0 (sept, 730 Hz). Anal. calcd. for C₇₂H₁₂₀F₆N₂P₆Zn₂: C, 55.49; H, 7.76; N, 1.80. Found: C, 54.91; H, 7.56; N, 1.77. UV-vis (THF, nm(M⁻¹cm⁻¹)): 302 (30 500), 334 sh.

Synthesis of [(^tBu₂-PNP)Zn]₂][OTf]₂ (4.6b): A solution of **4.4** (469 mg, 0.823) in THF (15 ml) was treated with excess (>5 equiv.) potassium hydride at which time the solution turned yellow and effervescence was observed. The reaction was stirred for 3 h and filtered to remove the unreacted potassium hydride. The filtrate was added to a sealable reaction bomb. Zn(OTf)₂ (300 mg, 0.823 mmol) was added as a solid and the bomb flask was sealed with a Teflon[®] plug. The reaction was heated to 75 °C for 24 h at

which time all of the $\text{Zn}(\text{OTf})_2$ had dissolved. The solvent was removed under reduced pressure and the residual off-white solids were washed with petroleum ether (2 x 10 mL) and dried thoroughly in vacuo. The white solids were dissolved in CH_2Cl_2 (8 mL), filtered through a glass micro-filter, and layered with petroleum ether (10 mL), affording analytically pure colorless crystals (422 mg, 70%) after 2 days. ^1H , ^{13}C NMR, and UV-vis were as reported for **4.6a**.

$^{31}\text{P}\{^1\text{H}\}$ NMR (121 MHz, CD_2Cl_2): δ -36.6 (s). Anal. calcd for $\text{C}_{74}\text{H}_{120}\text{F}_6\text{N}_2\text{O}_6\text{P}_4\text{S}_2\text{Zn}_2$: C, 56.06; H, 7.84; N, 1.82; Found: C, 56.38; H, 7.33; N, 1.95.

Synthesis of $[(^t\text{Bu}_2\text{-PNP})\text{Cu}]\{(^t\text{Bu}_2\text{-PNP})\text{Zn}\}[\text{PF}_6]$ (4.7**):** Quantities of **4.5** (89 mg, 0.064 mmol) and **4.6** (100 mg, 0.064) were combined in a 20 mL reaction vial with THF (10 mL), sealed with a Teflon cap, and stirred at 75 °C for 14 h. The pale yellow solution was evaporated to dryness under reduced pressure and the resultant pale yellow solids were washed with petroleum ether (20 mL). The solids were then redissolved in CH_2Cl_2 , the solution filtered, and the solvent removed from the filtrate *in vacuo* which afforded spectroscopically pure product (173 mg, 96%). Analytically pure crystals suitable for X-ray diffraction were obtained by vapor diffusion of petroleum ether into a concentrated solution of **4.7** in THF.

^1H NMR (500 MHz, CD_2Cl_2): δ 7.46 (m, 2H), 7.31 (m, 4H), 2.65 (m, 2H), 6.76 (m, 2H), 6.54 (m, 2H), 2.1-1.4 (m, 19 H), 1.04 (d, 12H), 0.94 (m, 5H), 0.86 (d, 6H), 0.83 (d, 6H), 0.80 (d, 6H), 0.76 (d, 6H), 0.71 (d, 6H), 0.62 (d, 6H). ^{13}C NMR (125.7 MHz, CD_2Cl_2): δ 164.6, 162.4, 145.7, 143.4, 131.3, 129.9, 129.1, 128.4, 127.2, 125.3, 117.6, 117.4, 38.7, 36.4, 35.6, 34.9, 34.7, 32.6, 31.8, 31.7, 26.4, 26.3, 26.0, 25.8, 25.6, 25.3, 25.1, 24.9. $^{31}\text{P}\{^1\text{H}\}$ NMR (121 MHz, CD_2Cl_2): δ -31.8 (s, P-Cu), -40.0 (s, P-Zn), -143.0 (sept, 730

Hz). Anal. calcd for $C_{72}H_{120}CuF_6N_2P_5Zn$: C, 61.26; H, 8.57; N, 1.98. Found: C, 61.48; H, 8.73; N, 1.73. UV-vis (THF, $nm(M^{-1}cm^{-1})$): 290 (21 600), 306 (23 400), 350 sh, 396 (7400).

Synthesis of $\{[(PNP)Cu]_2\}[B(C_6H_3(CF_3)_2)_4]$, 4.8: Complex 4.5 (150 mg, 0.144 mmol) and $[Cp_2Fe][B(C_6H_3(CF_3)_2)_4]$ (144 mg, 0.137 mmol) were combined in a 20 mL reaction vial and dissolved in CH_2Cl_2 (10 mL). The reaction immediately turned red-brown and stirring was continued for 30 min at which time the solvent was removed *in vacuo*. The resultant solids were washed with petroleum ether (2 x 10 mL), extracted into diethyl ether (7 mL), filtered through a glass micro-filter, and layered with petroleum ether. Analytically pure red crystals (203 mg, 78%) suitable for X-ray diffraction were obtained after two successive recrystallizations from diethyl ether/petroleum ether at -35 °C. Anal. calcd. for $C_{88}H_{100}BCu_2F_{24}N_2P_4$ C, 55.53; H, 5.30; N, 1.47; Found: C, 55.73; H, 5.21; N, 1.39. UV-vis (CD_2Cl_2 , $nm(M^{-1}cm^{-1})$): 260 (sh), 309 (14900), 359 (sh), 416 (2930), 529 (1090), 583 (sh), 661 (sh), 818 (1520), 981 (2053), 1684 (4500).

Synthesis of $[Cu(PNP)=(PNP)Cu][BF_4]_2$ (4.9): $NOBF_4$ (22.5 g, 0.192 mmol) and 4.3 (100 mg, 0.096 mmol) were combined in chlorobenzene and stirred for 18 h, after which the solution had become inky purple in color. The solution was filtered through a glass micro-filter and layered with petroleum ether. Upon standing for 4 days, analytically pure, X-ray quality crystals were obtained (86 mg, 74%). The room temperature NMR of the crystalline material is poorly resolved which is likely due to a fluxional interaction of the BF_4 counterion and the 16 e⁻ Cu centers. This is evident from very broad ^{19}F NMR resonances rather than the sharp signal that is expected for an uncoordinated anion.

^1H NMR (300 MHz, CD_2Cl_2): δ 8.7 (br d), 8.51 (br d), 8.2 (br d), 7.8-7.3 (m), 6.93 (s), 2.45-1.55 (m), 1.11 (d), 1.03 (d), 0.98-0.92 (m). ^{19}F NMR (282 MHz, CD_2Cl_2): δ -108.0 (br s), -125.5 (br s). $^{31}\text{P}\{^1\text{H}\}$ NMR (121 MHz, CD_2Cl_2): δ -27--31 (m), -32.8 (s). Anal. calcd. for $\text{C}_{56}\text{H}_{86}\text{B}_2\text{Cu}_2\text{F}_8\text{N}_2\text{P}_4$ C, 55.41; H, 7.31; N, 2.31. Found: C, 55.01; H, 7.38; N, 2.26. UV-vis (CD_2Cl_2 , $\text{nm}(\text{M}^{-1}\text{cm}^{-1})$): 293 (7370), 327 (sh), 570 (sh), 613 (16250).

Synthesis of $\{(\text{Bu}_2\text{-PNP})\text{Cu}\}_2[\text{B}(\text{C}_6\text{H}_3(\text{CF}_3)_2)_4]$ (4.10a): Complex **4.5** (134 mg, 0.106 mmol) and $[\text{Cp}_2\text{Fe}][\text{B}(\text{C}_6\text{H}_3(\text{CF}_3)_2)_4]$ (111 mg, 0.106 mmol) were combined in a 20 mL reaction vial and dissolved in diethyl ether (10 mL). The reaction immediately turned red-brown and stirring was continued for 12 h after which time the solvent was removed *in vacuo*. The resultant solids were washed with petroleum ether (2 x 10 mL), extracted with diethyl ether (7 mL), filtered through a glass micro-filter, and the filtrate layered with petroleum ether. Analytically pure red crystals (226 mg, 88%) suitable for X-ray diffraction were obtained after two days at $-35\text{ }^\circ\text{C}$.

$^{19}\text{F}\{^1\text{H}\}$ NMR (282 MHz, CD_2Cl_2): δ -60.2. Anal. Calcd. for $\text{C}_{104}\text{H}_{132}\text{BCu}_2\text{F}_{24}\text{N}_2\text{P}_4$: C, 58.70; H, 6.25; N, 1.32. Found: C, 58.34; H, 6.14; N, 1.41.

Synthesis of $\{(\text{Bu}_2\text{-PNP})\text{Cu}\}_2[\text{SbF}_6]$ (4.10b): Complex **4.5** (165 mg, 0.131 mmol) and AgSbF_6 (44.8 mg, 0.131 mmol) were combined in a 20 mL reaction vial and dissolved in THF (10 mL). The reaction immediately turned red-brown and stirring was continued for 12 h, after which time the solution was filtered through a glass micro-filter to remove the Ag^0 byproduct. The solvent was removed from the filtrate under reduced pressure, and the resultant red solids extracted into CH_2Cl_2 (4 mL), filtered and layered with petroleum ether. After two days, analytically pure red crystals (159 mg, 81%) were obtained. Anal. calcd. for $\text{C}_{72}\text{H}_{120}\text{Cu}_2\text{F}_6\text{N}_2\text{P}_4\text{Sb}$ C, 57.63; H, 8.06; N, 1.87; Found: C,

57.64; H, 8.03; N, 2.17. Evans' Method (CD_2Cl_2 , 298 K): 1.63 BM. UV-vis (CD_2Cl_2 , $\text{nm}(\text{M}^{-1}\text{cm}^{-1})$): 260 (sh), 312 (22 360), 377 (sh), 430 (3810), 510 (2280), 586 (sh), 639 (sh), 804 (1510), 941 (940), 1788 (5490).

Synthesis of $\{(\text{tBu}_2\text{-PNP})\text{Cu}\}_2[\text{SbF}_6]_2$ (4.11**):** Complex **4.5** (100 mg, 0.079 mmol) and NOSbF_6 (42 mg, 0.18 mmol) were combined in a 20 mL reaction vial and dissolved in CH_2Cl_2 (10 mL). Upon dissolution, solution immediately became red-brown in color then became blue after 10 min. After an additional 3 h of stirring the solution was concentrated to 3 mL, filtered through a glass micro-filter and layered with petroleum ether (15 ml). Cooling the mixture to $-35\text{ }^\circ\text{C}$ for 4 days caused a deep blue solid to precipitate. Two successive recrystallizations of **4.11** from petroleum ether/ CH_2Cl_2 at $-35\text{ }^\circ\text{C}$ afforded an analytically pure, blue microcrystalline solid (65 mg, 47%) suitable for X-ray diffraction studies. Modest yields result from multiple recrystallizations to insure purity and are not reflective of a low conversion to product.

Anal. calcd. for $\text{C}_{72}\text{H}_{120}\text{Cu}_2\text{F}_{12}\text{N}_2\text{P}_4\text{Sb}_2$: C, 49.81; H, 6.97; N, 1.61; Found: C, 49.41; H, 6.96; N, 1.76. Magnetic susceptibility (CD_2Cl_2 , 298 K): 1.69 BM. UV-vis (CD_2Cl_2 , $\text{nm}(\text{M}^{-1}\text{cm}^{-1})$): 294 (16 500), 321 (sh), 346 (21700), 426 (sh), 510 (sh), 574 (sh), 620 (12 900), 1297 (300).

IV.E. References Cited

¹ (a) Kato, M., Johnassen, H. B.; Fanning, J. C.; *Chem. Rev.* **1964**, *64*, 99. (b) Kato, M.; Muto, Y.; *Coord. Chem Rev.* **1988**, *92*, 45. (c) Kahn, O.; *Angew. Chem. Int. Ed. Eng.* **1985**, *24*, 834.

² (a) *Bioinorganic Chemistry of Copper*; Karlin, K. D.; Tyeklar, Z.; Eds.; Chapman & Hall: New York, N.Y., **1993**. (b) *Bioinorganic Chemistry*; Bertini, I.; Gray, H. B.; Lippard, S. J.; Valentine, J. S. University Science Books: Mill Valley, CA, **1994**.

³ (a) Elliott, C. M.; Pichot, F.; Bloom, C. J.; Rider, L. S. *J. Am. Chem. Soc.* **1998**, *120*, 6781. (b) Bargossi, C.; Fiorini, M. C.; Montalti, M.; Prodi, L.; Zaccheroni, N. *Coord. Chem. Rev.* **2000**, *208*, 17. (c) de Silva, A. P.; Fox, D. B.; Huxley, A. J. M.; Moody, T. S. *Coord. Chem. Rev.* **2000**, *205*, 41. (d) Drummond, T. G.; Hill, M. G.; Barton, J. K. *Nat. Biotech.* **2003**, *21*, 1192. (e) Sutin, N.; Creutz, C. *Pure & Appl. Chem.* **1980**, *52*, 2717.

⁴ (a) Vallee, B. L.; Williams, R. J. P. *Proc. Natl. Acad. Sci. U.S.A.* **1968**, *59*, 498. (b) Williams, R. J. P. *Inorg. Chim. Acta Rev.* **1971**, *5*, 137. (c) Williams, R. J. P. *Eur. J. Biochem.* **1995**, *234*, 363. (d) Hathaway, B. J.; Billing, D. E. *Coord. Chem. Rev.* **1970**, *5*, 143. (e) Hathaway, B. J. *Coord. Chem. Rev.* **1981**, *35*, 211.

⁵ (a) Chen, P.; Gorelsky, S. I.; Ghosh, S.; Solomon, E. I.; *Angew. Chem. Int. Ed.* **2004**, *43*, 4132. (b) Rosenzweig, A. C. *Nat. Struct. Biol.* **2000**, *7*, 169. (c) Zumft, W.G. *Microbiol. Mol. Biol. Rev.* **1997**, *61*, 533.

⁶ (a) Lieberman, R. L.; Rosenzweig, A. C. *Nature* **2005**, *434*, 177. (b) Lieberman, R. L.; Shrestha, D. B.; Doan, P. E.; Hoffman, B. M.; Stemmler, T. L.; Rosenzweig, A. C. *Proc. Natl. Acad. Sci. U.S.A.* **2003**, *100*, 3820.

⁷ (a) Ferguson-Miller, S.; Babcock, G. T. *Chem. Rev.* **1996**, *96*, 2889. (b) Gamelin, D. R.; Randall, D. W.; Hay, M. T.; Houser, R. P.; Mulder, T. C.; Canters, G. W.; de Vries, S.; Tolman, W. B.; Lu, Y.; Solomon, E. I. *J. Am. Chem. Soc.* **1998**, *120*, 5246. (c) George, S. D.; Metz, M.; Szilagyi, R. K.; Wang, H. X.; Cramer, S. P.; Lu, Y.; Tolman, W. B.; Hedman, B.; Hodgson, K. O.; Solomon, E. I. *J. Am. Chem. Soc.* **2001**, *123*, 5757. (d) Ramirez, B. E.; Malmstrom, B. G.; Winkler, J. R.; Gray, H. B. *Proc. Natl. Acad. Sci. U.S.A.* **1995**, *92*, 11949.

⁸ (a) Kroneck, P. M. H.; Antholine, W. E.; Riester, J.; Zumft, W. G. *FEBS Lett.* **1989**, *248*, 212. (b) Kroneck, P. M. H.; Antholine, W. E.; Riester, J.; Zumft, W. G. *FEBS Lett.* **1988**, *242*, 70. (c) Antholine, W. E.; Kastrau, D. H. W.; Steffens, G. C. M.; Buse, G.; Sumft, W. G.; Kroneck, P. M. H. *Eur. J. Biochem.* **1992**, *209*, 875.

⁹ (a) Houser, R. P.; Young, V. G., Jr.; Tolman, W. B. *J. Am. Chem. Soc.*, **1996**, *118*, 2101. (b) Blackburn, N. J.; deVries, S.; Barr, M. E.; Houser, R. P.; Tolman, W. B.; Sanders, D.; Fee, J. A. *J. Am. Chem. Soc.* **1997**, *119*, 6135. (c) Hagadorn, J. R.; Zahn, T. I.; Que, L., Jr.; Tolman, W. B. *J. C. S. Dalton Trans.* **2003**, 1790.

¹⁰ Al-Obaidi, A.; Baranovič, G.; Coyle, J.; Coates, C. G.; McGarvey, J. J.; McKee, V.; Nelson, J. *Inorg. Chem.* **1998**, *37*, 3567.

¹¹ (a) LeCloux, D. D.; Davydov, R.; Lippard, S. J. *Inorg. Chem.* **1998**, *37*, 6814. (b) LeCloux, D. D.; Davydov, R.; Lippard, S. J. *J. Am. Chem. Soc.* **1998**, *120*, 6810. (c) He, C.; Lippard, S. J. *Inorg. Chem.* **2000**, *39*, 5225.

¹² Gupta, R.; Zhang, Z. H.; Powell, D.; Hendrich, M. P.; Borovik, A. S. *Inorg. Chem.*, **2002**, *41*, 5100.

- ¹³ Snyder, B. S.; Patterson, G. S.; Abrahamson, A. J.; Holm, R. H.; *J. Am. Chem. Soc.* **1989**, *111*, 5214.
- ¹⁴ Harkins, S. B.; Peters, J. C. *J. Am. Chem. Soc.* **2005**, *127*, 2030.
- ¹⁵ (a) Glazer, E. C.; Magde, D.; Tor, Y.; *J. Am. Chem. Soc.* **2005**, *127*, 4190. (b) Browne, W. R.; O'Boyle, N. M.; Henry, W.; Guckian, A. L.; Horn, S.; Fett, T.; O'Connor, C. M.; Duati, M.; De Cola, L.; Coates, C. G.; Ronayne, K. L.; McGarvey, J. J.; Vos, J. G.; *J. Am. Chem. Soc.* **2005**, *127*, 1229. (c) Zhou, Z.; Fahrni, C. J.; *J. Am. Chem. Soc.* **2004**, *126*, 8862.
- ¹⁶ Ford, P. C.; Cariati, E.; Bourassa, J. *Chem. Rev.* **1999**, *99*, 3625.
- ¹⁷ McMillin, D. R.; McNett, K. M. *Chem. Rev.* **1998**, *98*, 1201.
- ¹⁸ Roundhill, D. M. *Photochemistry and Photophysics of Metal Complexes*; Fackler, J. P., Jr.; In *Modern Inorganic Chemistry*; Plenum Press: New York, NY, 1994; pp 49 & 165.
- ¹⁹ Cuttell, D. G.; Kuang, S.-M.; Fanwick, P. E. McMillin, D. R.; Walton, R. A. *J. Am. Chem. Soc.* **2002**, *124*, 6.
- ²⁰ Harkins, S. B.; Peters, J. C. *J. Am. Chem. Soc.* **2004**, *126*, 2885.
- ²¹ (a) Robin, M. B.; Day, P. *Adv. Chem. Phys.*, **1967**, *10*, 247. (b) Day, P. *Endeavour* **1970**, *29*, 45.
- ²² {(SNS)Cu^I}₂: CCDC 234450; [{(SNS)Cu^{1.5}}₂]⁺: CCDC 234451; *Cambridge Structural Database*; Cambridge, England (accessed May 28, 2005).
- ²³ Peters, J. C.; Harkins, S. B.; Brown, S. D.; Day, M. W. *Inorg. Chem.* **2001**, *40*, 5083.
- ²⁴ Liang, L.-C.; Lin, J.-M.; Hung, C.-H. *Organometallics* **2003**, *15*, 3007.
- ²⁵ Ozerov, O. V.; Guo, C.; Papkov, V. A.; Foxman, B. M.; *J. Am. Chem. Soc.* **2004**, *126*, 4792.

-
- ²⁶ Tsuda, T.; Yazawa, T.; Watanabe, K.; Fuji, T.; Saegusa, T. *J. Org. Chem.* **1981**, *46*, 192
- ²⁷ Drago, R. S. *Physical Methods for Chemists*, 2nd ed.; Surfside Scientific Publishers: Gainesville, FL, 1992.
- ²⁸ Shannon, R. D.; *Acta. Cryst.* **1976**, *A32*, 751.
- ²⁹ Che, C.-M.; Mao, Z.; Miskowski, V. M.; Tse, M.-C.; Chan, C.-K.; Cheung, K.-K.; Philips, D. L.; Leug, K.-H. *Angew. Chem. Int. Ed.* **2000**, *39*, 4084.
- ³⁰ Parameters for electrochemical experiments: Pt working electrode, AgNO₃/Ag non-aqueous reference, Pt wire auxillary, 0.35 M tetrabutylammonium hexafluoroborate in THF, 200 mV/sec. It was necessary to switch to a Pt working electrode from glassy carbon to attenuate the formation of surface adsorbed species due to the highly non-polar nature of the analyte.
- ³¹ Smith, M. B.; March, J. *March's Advanced Organic Chemistry*, 5th Ed. John Wiley & Sons, Inc.: New York, NY, 2001.
- ³² Complexes **4.9** and **4.11** can also prepared by the one electron oxidation of **4.8** or **4.10b**, however, we find the two electron oxidation route from **4.3** or **4.5** to be preferable.
- ³³ THF was found to be suitable for electrochemistry which is attributed to modest stability of the dimeric, doubly oxidized product of **4.3** prior to decomposition to **4.9**.
- ³⁴ Seidal, B.; Hammond, G. S.; *J. Org. Chem.* **1963**, *28*, 3280.
- ³⁵ (a) Chaudhuri, P.; Hess, M.; Müller, J.; Hildenbrand, K.; Bill, E.; Weyhermüller, T.; Wieghardt, K. *J. Am. Chem. Soc.* **1999**, *121*, 9599. (b) Shultz, D. A.; Vostrikova, K. E.; Bodnar, S. H.; Koo, H.-J.; Whangbo, M.-H.; Kirk, M. L.; Depperman, E. C.; Kampf, J. W. *J. Am. Chem. Soc.* **2003**, *125*, 1607. (c) Bill, E.; Müller, J.; Weyhermüller, T.;

Wieghardt, K. *Inorg. Chem.*; **1999**, *38*, 5795. (d) Min, K. S.; Weyhermüller, T.; Bothe, E.; Wieghardt, K. *Inorg. Chem.*; **2004**, *43*, 5795.

³⁶ Harkins, S. B.; Peters, J. C.; Facial Coordination of a Pincer-like Amido Complex of Platinum(IV) Generated by Photoisomerization. *Inorg. Chem. to be submitted for publication.*

³⁷ The structural inequivalency between the copper centers was also found in the crystal structure of the bis-[PF₆]⁻ salt of **4.11**. *Unpublished results.*

³⁸ Discreet mononuclear Cu^{II} complexes supported by ligands **4.1** or **4.4** have not been prepared because of the reducing nature of the phosphine ligands. However, characteristic four-line hyperfine splitting patterns characteristic of a Cu^{II} are easily discernable in the previously described (SNS)Cu^{II}Cl complex.

³⁹ *Magnetochemistry*; Carlin, R. L.; Springer-Verlag: Heidelberg, Germany, 1986.

⁴⁰ Fernandez, C. O.; Cricco, J. A.; Slutter, C. E.; Richards, J. H.; Gray, H. B.; Vila, A. J. *J. Am. Chem. Soc.*; **2001**, *123*, 11678.

⁴¹ (a) Sur, S. K. *J. Magn. Reson.* **1989**, *82*, 169. (b) Evans, D. F. *J. Chem. Soc.* **1959**, 2003.

⁴² *Electron Paramagnetic Resonance : Elementary Theory and Practical Applications*, Weil, J. A.; Bolton, J. R.; Wertz, J. E.; Wiley Interscience: New York, N.Y., 1994.

⁴³ *Molecular Magnetism*, Kahn, O.; VCH Publishers, Inc.: New York, N.Y., 1993.

⁴⁴ *Electron Paramagnetic Resonance of Exchange Coupled Systems*, Bencini, A.; Gatteschi, D.; Springer-Verlag: Berlin, Germany, 1990.

⁴⁵ Ribas, X.; Jackson, D. A.; Donnadiou, B.; Mahia, J.; Parella, T.; Xifra, R.; Hedman, B.; Hodgson, K. O.; Llobet, A.; Stack, T. D. P. *Angew. Chem., Int. Ed.* **2002**, *41*, 2991.

-
- ⁴⁶ (a) Whittaker, J. W. *Chem. Rev.* **2003**, *103*, 2347. (b) DuBois, J. L.; Mukherjee, P.; Stack, T.D.P.; Hedman, B.; Solomon, E. I.; Hodgson, K. O. *J. Am. Chem. Soc.* **2000**, *122*, 5775.
- ⁴⁷ Krebs, C.; Glaser, T.; Bill, E.; Weyhermüller, T.; Meyer-Klaucke, W.; Wieghardt, K.; *Angew. Chem. Int. Ed.* **1999**, *38*, 359.
- ⁴⁸ a) Klemm, W.; Huss, E.; *Z. Anorg. Chem.* **1949**, *259*, 221.; b) Hoppe, R.; *Angew. Chem.* **1950**, *62*, 339.
- ⁴⁹ (a) Gerloch, M.; Slade, R.C.; *J. Chem. Soc. A.* **1969**, 1012. (b) *Advanced Inorganic Chemistry*, Cotton, F. A.; Wilkinson, G.; John Wiley & Sons, New York, N.Y., 1988.
- ⁵⁰ Bates, C. A.; *Proc. Phys. Soc.*, **1962**, *79*, 69.
- ⁵¹ Neese, F.; *J. Chem. Phys.* **2005**, *122*, 34107.
- ⁵² Perich, J. W.; Johns, R. B. *Synthesis* **1988**, *2*, 142.
- ⁵³ Zhao, H.; Tanjutco, C.; Thayumanavan, S. *Tet. Lett.* **2001**, *42*, 4421.
- ⁵⁴ Chávez, I.; et al. *J. Organomet. Chem.* **2000**, *601*, 126.
- ⁵⁵ O'Connor, C. J.; *Prog. Inorg. Chem.* **1982**, *29*, 203.
- ⁵⁶ Wenger, O. S.; Henling, L. M.; Day, M. W.; Winkler, J. R.; Gray, H. B.; *Inorg. Chem.*, **2004**, *43*, 2043.
- ⁵⁷ Lyubovitsky, J. G.; Gray, H. B.; Winkler, J. R.; *J. Am. Chem. Soc.* **2002**, *124*, 5481.
- ⁵⁸ Lee, J. C.; Engman, K. C.; Tezcan, F. A.; Gray, H. B.; Winkler, J. R.; *Proc. Natl. Acad. Sci. U.S.A.* **2002**, *99*, 14778.
- ⁵⁹ Demas, J. N.; Crosby, G. A. *J. Phys. Chem.* **1971**, *75*, 991.
- ⁶⁰ Rabinowitz, R.; Pellon, J.; *J. Org. Chem.* **1961**, *26*, 1961.